Development of a dataset on the in-plane experimental response of URM piers with bricks and blocks

Morandi, P.; Albanesi, L.; Graziotti, F.; Li Piani, T.; Penna, A.; Magenes, G.

DOI
10.1016/j.conbuildmat.2018.09.070

Publication date
2018

Document Version
Accepted author manuscript

Published in
Construction and Building Materials

DEVELOPMENT OF A DATASET ON THE IN-PLANE EXPERIMENTAL RESPONSE OF URM PIERS WITH BRICKS AND BLOCKS

P. Morandi[a,b,*], L. Albanesi[b], F. Graziotti[a,b], T. Li Piani[c], A. Penna[a,b], G. Magenes[a,b]

[a] *University of Pavia, Department of Civil Engineering and Architecture - DICAr, via Ferrata 3, Pavia, Italy*.

[b] *European Centre for Training and Research in Earthquake Engineering - EUCENTRE, via Ferrata 1, Pavia, Italy*.

[c] TU Delft, *Faculty of Civil Engineering and Geoscience, Applied Mechanics, Stevinweg 1, Delft, The Netherlands.*

E-mail addresses: paolo.morandi@unipv.it (P. Morandi), luca.albanesi@eucentre.it (L. Albanesi), francesco.graziotti@unipv.it (F. Graziotti), t.lipiani@tudelft.nl (T. Li Piani), andrea.penna@unipv.it (A. Penna), guido.magenes@unipv.it (G. Magenes).

ABSTRACT

In this paper, a dataset collecting the results of in-plane cyclic tests on unreinforced masonry piers, carried out within different research projects, is presented. The dataset includes brick and block walls with different materials, bed-and head-joint typologies, dimensions, boundary conditions and vertical applied loads. The development of such dataset aims at providing a tool for the improvement of the understanding and the evaluation of the main parameters that may influence and govern the lateral response of the URM piers under seismic excitation. A preliminary investigation on the in-plane lateral strength and displacement capacity, being two of the most significant parameters used in seismic analyses for the design and assessment of masonry buildings, has been proposed. The dataset, that already groups several specimens, is freely shared and might be continuously updated. This source of information of consistent and reliable test results represents a necessary step into the process of definition of shared rules within the scientific and technical community, in particular for the improvement of codified criteria, analytical and numerical models and testing procedures.

KEYWORDS

URM piers; bricks and blocks; in-plane cyclic tests; dataset; lateral strength; displacement capacity.

1. INTRODUCTION

The presence of existing and modern buildings with loadbearing structures constituted by unreinforced masonry walls with bricks and blocks is largely widespread in Europe and around the world, even in areas with considerable seismic hazard, since it is still a competitive choice for low-rise residential buildings from many points of view, not necessarily all related to the structural response. Nevertheless, despite the huge effort devoted to the evaluation of analytical and experimental in-plane response of URM piers, a complete understanding of all the involved phenomena is still lacking.

For these reasons, a statistically significant dataset that assembles the essential information and the results of in-plane cyclic tests on unreinforced masonry walls may provide a useful tool to improve the current analytical models and the main seismic parameters that govern the lateral response. Analyses of the dataset may also serve as reference for revisions of the code recommendations. In addition, this work may constitute a possible guide for testing procedures and protocols for future experimental campaigns in terms of minimum needed information and well-posed criteria, that can offer a more rigorous and consistent approach to plan and process the test results. Finally, although static and dynamic numerical analyses are necessary to evaluate the vulnerability of a single structure (e.g., Mallardo et al. [24]) or an entire building stock (e.g., Crowley et al. [25]), there is still a lack in numerical models in capturing the actual response of masonry buildings, especially when subjected to cyclic and dynamic loading, as in the case of blind predictions of experimental tests on shaking table or simulation of damage diffusion on structures hit by earthquakes (e.g., Kallioras et al. [26]). This dataset can also be an important source for the development of more accurate numerical micro- (e.g., Adam et al. [27]; Gabor et al. [28]) and macro-models (e.g., Magenes et al. [29]; Lagomarsino et al. [30]) for seismic design and assessment of masonry buildings.

Therefore, a dataset assorting the results of 188 in-plane cyclic tests unreinforced masonry piers, carried out mainly in Europe within different research projects, has been here developed. It contains information on tests performed on specimens with different construction masonry technologies with bricks and blocks (clay, calcium silicate, aerated autoclaved concrete and lightweight aggregate concrete), bed-and head-joint types, dimensions, boundary conditions, vertical applied loads and horizontal loading history. The failure modes obtained in the tests cover several cases, flexural/rocking, pure shear as well as hybrid modes. Table 1 indicates the institution involved in the tests, the number of the performed in-plane cyclic tests and the materials of the masonry specimens.

Table 1. List of sources. For the abbreviations of the masonry types refer to Table 3.

University / Institution	N. of Test	Masonry type
University of Pavia [1]	*20*	*CS, HC, LAC*
University of Pavia [2]	*4*	*SB-C*
JRC, Ispra [3]	*2*	*SB-C*
University of Illinois, Urbana-Champaigne [4]	*3*	*SB-C*
ZAG, Ljubljana [5]	*13*	*SB-C*
University of Colorado, Boulder [6]	*3*	*SB-C*
ZAG, Ljubljana [7]	*22*	*HC*
Technical University of Munich [8]	*3*	*CS, HC*
University of Kassel [9]	*25*	*HC, CS, LAC*
University of Dortmund [10]	*11*	*CS, AAC, HC, LAC*
EUCENTRE, Pavia [11]	*1*	*AAC*
EUCENTRE, Pavia [12]	*6*	*AAC*
EUCENTRE, Pavia [13]	*4*	*AAC*
EPFL, Lausanne [14]	*6*	*HC*
University of Padova [15]	*10*	*HC*
Technical University of Civil Engineering Bucharest [16]	*9*	*HC*
EUCENTRE, Pavia [17]	*5*	*HC*
EUCENTRE, Pavia [18]	*6*	*HC*
University of Kassel [19]	*13*	*AAC*
ETH, Zurich [20]	*10*	*CS, HC*
EUCENTRE, Pavia [21]	*5*	*HC*
EUCENTRE, Pavia [22]	*2*	*SB-CS*
EUCENTRE, Pavia [23]	*5*	*SB-C*

Attempts to build a systematic dataset with results of in-plane tests on masonry walls have been recently made, for example, by Augenti et al. [31], Salmanpour et al. [32], Gams et al. [33] and Vanin et al. [34]. In this work, the main novel aspects are attributable to the high number of large-scale specimens collected and, above all, to the development of a dataset that only includes those tests with sufficient documentation and that guarantees the requirement of consistency and completeness of the available data on units, mortar, masonry, tests of characterization, damage pattern and cyclic response. The dataset, that at the present stage already groups several specimens, can be freely downloaded [35], it will be continuously updated with new and past test results and it will be part of the European Masonry Database in collaboration with other research institutions.

Although in this paper some key aspects related to the in-plane lateral strength, failure modes and displacement capacity at different limit states have been investigated, the largest effort has been devoted to the preparation of the dataset itself, which is mainly intended to provide a tool available for future studies aiming at the improvement of the understanding of the in-plane performance and modelling of URM walls.

2. FRAMEWORK OF THE DATASET

The dataset collects the results of URM piers subjected to in-plane cyclic tests constituted of different masonry materials (with bricks and blocks), bed-and head-joint typologies, dimensions, boundary conditions, vertical applied loads and horizontal loading history. A total of 188 piers forms the complete list, including 101 hollow clay with vertical perforation, 11 lightweight aggregate concrete with vertical perforation, 18 solid unit calcium silicate, 26 solid unit autoclaved aerated concrete and 32 solid brick (30 clay and 2 calcium silicate) masonry piers. General purpose or thin layer mortar bed-joints and different types of head-joints (completely filled, filled with thin layer mortar, filled in the pocket, unfilled with plain or tongue and groove units) characterize the masonry walls with blocks. The clay and calcium-silicate solid brick masonry is instead realized with general-purpose mortar. The height of the piers ranges from 1.17 m to 3.00 m. The majority of the tests are conducted with "Cantilever" and "Double Fixed" boundary conditions, with exception of few specimens performed with intermediate conditions. Values of the vertical applied stress over the compressive strength ratio (σ_v/f) ranging between 2% and 41% are found. The failure modes obtained in the tests cover several cases from flexural/rocking to pure shear with diagonal or step-wise cracking involving the joints and the units, sliding at the ends of the piers, "gaping" with stepped cracking, and hybrid modes with the occurrence of two different failure modes, as schematically reported in Figure 1.

All the considered in-plane shear tests were conducted applying, initially, a vertical load and, consequently, a cyclic horizontal load at the upper part of the wall. The horizontal action was applied in the form of programmed displacements, cyclically imposed in both directions with step-wise increased amplitudes up to ultimate conditions of the specimens; at each displacement amplitude, the loading was repeated two times (i.e., at the UTCB of Bucharest [16] and EPFL of Lausanne [14]) or three (for the other research units). An example of a typical loading history and of a test set-up is shown in Figure 2. During the tests, forces and displacements acting on the walls were measured and hysteresis loops recorded. The positive "+" direction is set, conventionally, when the forces and the displacements of the acquired Force-Displacement curves lie in the first quadrant and negative "-" when lie in the third quadrant.

In addition, the available results of tests of characterization on units, mortar and masonry performed in the different experimental campaigns are also reported.

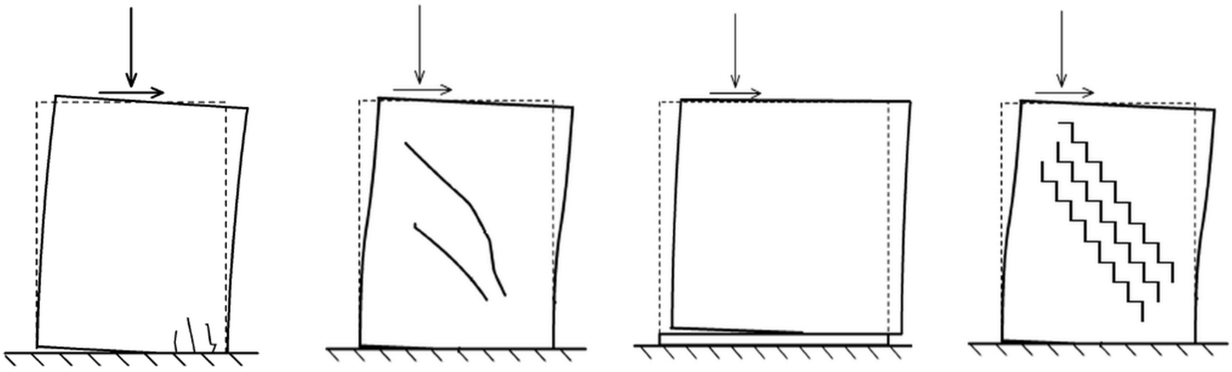

(a) (b) (c) (d)

Figure 1. Schemes of the most typical failure modes: (a) flexural/rocking; (b) shear with diagonal or step-wise cracking; (c) sliding at the base; (d) "gaping" with stepped cracking [18].

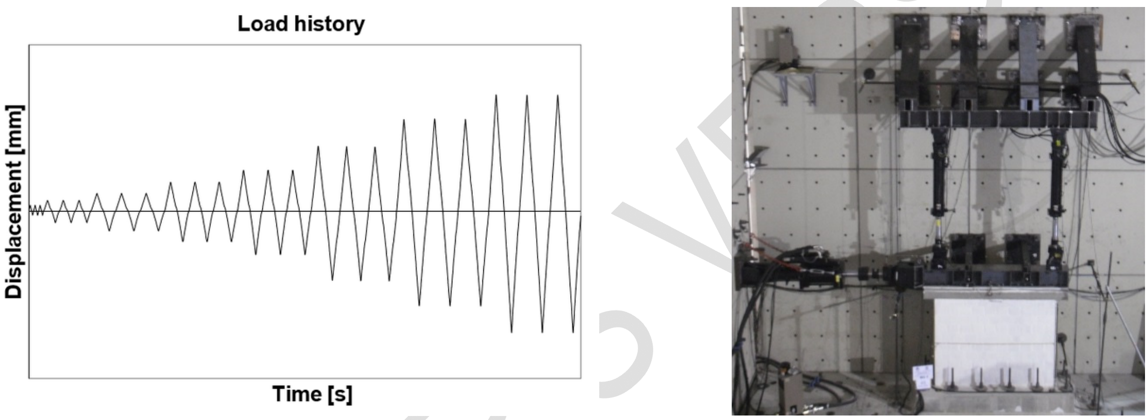

(a) (b)

Figure 2. (a) Loading history in cyclic tests; (b) test set-up at the EUCENTRE of Pavia [17].

The dataset is organized in eight sections with seventy-two columns of data in addition to the first one containing the sequential number of the specimens. The eight sections regard general information and reference [I], information on masonry type, units and mortar [II], information on masonry walls [III], test conditions [IV], calculated lateral resistances [V], experimental results through cyclic tests [VI], parameters of the bilinear curves [VII] and drift capacities [VIII]. All the data and parameters included in the different sections are summarized in Table 2, whereas Table 3 indicates the abbreviations used for the masonry types, the mortar joints, the test boundary conditions and the failure modes.

In the case of values or characteristics not available or not obtainable through calculation, a sign "/" has been inserted in the cells. In the header row of the dataset, the cells highlighted in blue indicate that the columns contain values derived from calculation.

Additional information on the characteristics of units, mortar and masonry and on the results and standards of further tests of characterization may be requested to the authors.

Table 2. Parameters used in the dataset

General info [I]	*Source*	Report, project, publication
	Specimen	Specimen name (original)
Information on masonry type, units and mortar [II]	*Material*	Material of masonry unit
	l_u [mm]	Unit length
	w_u [mm]	Unit width
	h_u [mm]	Unit height
	Void ratio [%]	Percentage of voids
	Unit density [kg/m^3]	Density of units
	f_b [MPa]	Unit mean compressive strength
	d [-]	Shape factor
	$f_{b,norm}$ [MPa]	Unit normalized compr. strength
	Bed-joints	Type of mortar bed-joints (“TL”, “GP”)
	Head-joints	Type of mortar head-joints (“F”, “TF”, “MP”, “U”, “UTG”)
	Strength class	Mortar strength class
	f_m [MPa]	Mortar mean compressive strength
Information on masonry walls (mean values) [III]	l [m]	Wall length
	t [m]	Wall thickness
	h [m]	Wall height
	h/l [-]	Wall height/length ratio
	n° of layers	Number of unit courses
	G [MPa]	Masonry shear modulus
	E [MPa]	Masonry elastic modulus
	f [MPa]	Masonry compressive strength
	f_{v0} [MPa]	Masonry initial shear strength
	μ [-]	Masonry friction coefficient
	f_t [MPa]	Masonry diagonal tensile strength
Test conditions [IV]	*Boundary conditions*	Test boundary conditions (“DF”, “C”, “O”)
	h_0/h [-]	Shear span ratio
	σ_v [MPa]	Applied vertical stress
	σ_v/f [-]	Vert. stress/compr. strength ratio
Calculated resistances [V]	M_u [kNm]	Resistant bending moment
	$f_{v,lim}$ [MPa]	Shear strength limit from EC6
	V_{flex} [kN]	Shear strength at flexure
	$V_{shear,i}$ [kN]	Shear strength from EC6
	$V_{shear,min}$ [kN]	Lower shear strength ($0.4 \cdot N$)
	$V_{shear,max}$ [kN]	Upper shear strength ($f_{vd} \cdot t \cdot l$)
Calculated resistances [V]	V_{shear} [kN]	$= V_{shear,min} \leq V_{shear,i} \leq V_{shear,max}$
	$V_{shear,lim,i}$ [kN]	Shear strength limit from EC6
	$V_{shear,lim,max}$ [kN]	Upper shear strength limit ($f_{v,lim} \cdot t \cdot l$)
	$V_{shear,lim}$ [kN]	$=\min(V_{shear,lim,i};\ V_{shear,lim,max})$
	V_{pred} [kN]	$=\min(V_{flex};\ V_{shear};\ V_{shear,lim})$
	Expected failure	Expected failure mode (“F” = flexural or “S” = shear)
Experimental results (cyclic tests) [VI]	*Fail. mode*	Observed failure mode
	↓	Comparison between expected and test failure mode (coloured)
	ξ range	Measure of dissipated energy
	δ_{cr} [mm]	Displ. at first visible crack
	$V_{max,exp}^+$ [kN]	Max. pos. experimental force
	$V_{max,exp}^-$ [kN]	Max. neg. experimental force
	$V_{pred}/V_{max,exp}$ [-]	Analytical/max. exp. force
	$\delta_{Vmax,exp}^+$ [mm]	Displ. at max. positive force
	$\delta_{Vmax,exp}^-$ [mm]	Displ. at min. positive force
	$\delta_{max,f}^+$ [mm]	Max. pos. displ. at all completed cycles
	$\delta_{max,f}^-$ [mm]	Max. neg. displ. at all completed cycles
	δ_{max}^+ [mm]	Max. positive displacement
	δ_{max}^- [mm]	Max. negative displacement
Parameters bilinear curves [VII]	k_{el}^+ [kN/mm]	Stiffness in positive direction
	k_{el}^- [kN/mm]	Stiffness in negative direction
	V_u^+ [kN]	Positive force of the plateau
	V_u^- [kN]	Negative force of the plateau
	δ_e^+ [mm]	Positive displ. at yield
	δ_e^- [mm]	Negative displ. at yield
	δ_u^+ [mm]	Positive displ. at $0.8 \cdot V_u^+$
	δ_u^- [mm]	Negative displ. at $0.8 \cdot V_u^-$
	μ_u^+ [-]	δ_u^+/δ_e^+
	μ_u^- [-]	δ_u^-/δ_e^-
	μ [-]	$\mathrm{Min}(\mu_u^+,\ \mu_u^-)$
Drift capacities [VIII]	θ_{cr} [%]	Drift at first crack
	θ_e [%]	Drift at elastic limit
	θ_{Vmax} [%]	Drift at peak force
	θ_u [%]	Drift at $0.80 \cdot V_u$
	$\theta_{max,f}$ [%]	Max. drift at all completed cycles
	θ_{max} [%]	Max. drift

Table 3. Abbreviations used in the dataset for the masonry unit types, the mortar joints, the test boundary conditions and the failure modes.

Masonry unit types	*HC*	Hollow clay (with vertical perforation)
	AAC	Autoclaved aerated concrete
	CS	Calcium silicate
	LAC	Lightweight aggregate concrete (with vertical perforation)
	SB-C	Solid clay (brick)
	SB-CS	Solid calcium silicate (brick)
Bed-joints	*GP*	General purpose
	TL	Thin layer
Head-joints	*F*	Filled (general purpose)
	TF	Thin filled
	MP	Mortar pocket
	UTG	Unfilled (tongue and groove)
	U	Unfilled
Static scheme	*DF*	Double fixed
	C	Cantilever
	O	Other boundary conditions
Experimental failure modes	*F*	Flexure
	S	Shear
	H-_ _	Hybrid (followed by the two main mechanisms involved)
	G	Gaping
	SL	Sliding (at the first or last course of the wall)
	D	Uncertain

2.1 General information and reference

The first section of the dataset contains two columns that specify the source of the data. In the first column, each University or involved institution is accompanied by the reference to the original publication or report and, in the second column, the original name of each specimen, as referred in the referenced documents, are reported.

2.2 Information on masonry type, units and mortars

The second section contains thirteen columns, reporting the main information about the masonry material type, the units and the mortar. The column #1 reports the blocks or bricks materials constituting of the masonry; four different materials are included in the dataset: clay (hollowed units "HC" and solid bricks "SB-C"), calcium silicate (solid blocks "CS" and bricks "SB-CS"), lightweight aggregate concrete "LAC", autoclaved aerated concrete "AAC". Figure 3 shows the composition of the dataset in terms of the masonry material of the tested specimens.

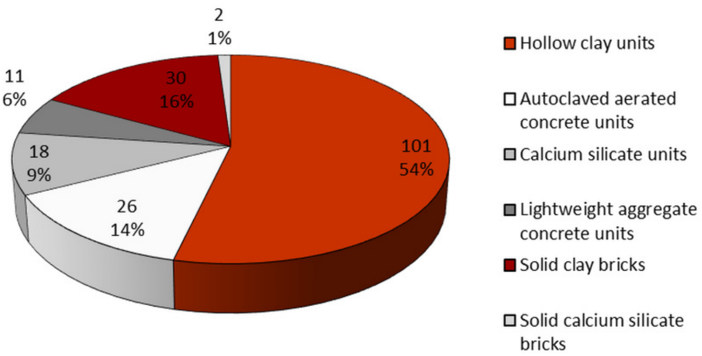

Figure 3. Masonry materials of the specimens included in the dataset.

The following three columns (#2, #3 and #4) report the unit dimensions (length l_u, width w_u and height h_u); column #5 contains the information about the void ratio (volume of any holes in percentage of the gross volume), being the experimental or the nominal value, in the case of hollow blocks, and the word "solid", in the case of solid units or bricks. The column #6 reports the gross density of the units (weight over gross volume of the units). The column #7, #8 and #9 are dedicated to the vertical compression strength of the units; in particular the experimental mean value of the unit strength, f_b, and the normalized one, $f_{b,norm}$, are reported respectively in column #7 and #9, being the latter written in grey when not available by the original sources and thus calculated as $f_b \cdot d$, where d is the shape factor depending on the geometry of the units (see EN 772-1 [36], reported in column #8).

The last four columns (from #10 to #13) of this section summarize the information on the mortar, with reference to the type of bed- and head-joints. In order to provide a homogeneous classification, a distinction between "general purpose" ("GP", mortar joint thickness between 10 and 15 mm) and "thin layer" bed-joints ("TL", mortar joint thickness between 0.5 and 3.0 mm) has been made, whereas the head-joint typologies are characterized by cases with general purpose filled mortar "F", thin filled mortar "TF", mortar in the pocket "MP", unfilled with plain units "U" and unfilled with tongue and groove units "UTG". Additionally, the declared mortar strength class according to EN 998-2 [37], if available, and the mean value of compression strength of mortar f_m, evaluated from experimental characterization tests (in black) or estimated in relation to the mortar class (in grey) are reported. Figure 4 shows the head- and the bed-joint typologies for the different masonry walls. In the case of lightweight aggregate concrete specimens, only tongue and groove units with unfilled head-joints are found (5 with general purpose and 6 with thin layer bed-joints), whereas general purpose mortar characterizes the solid brick masonry.

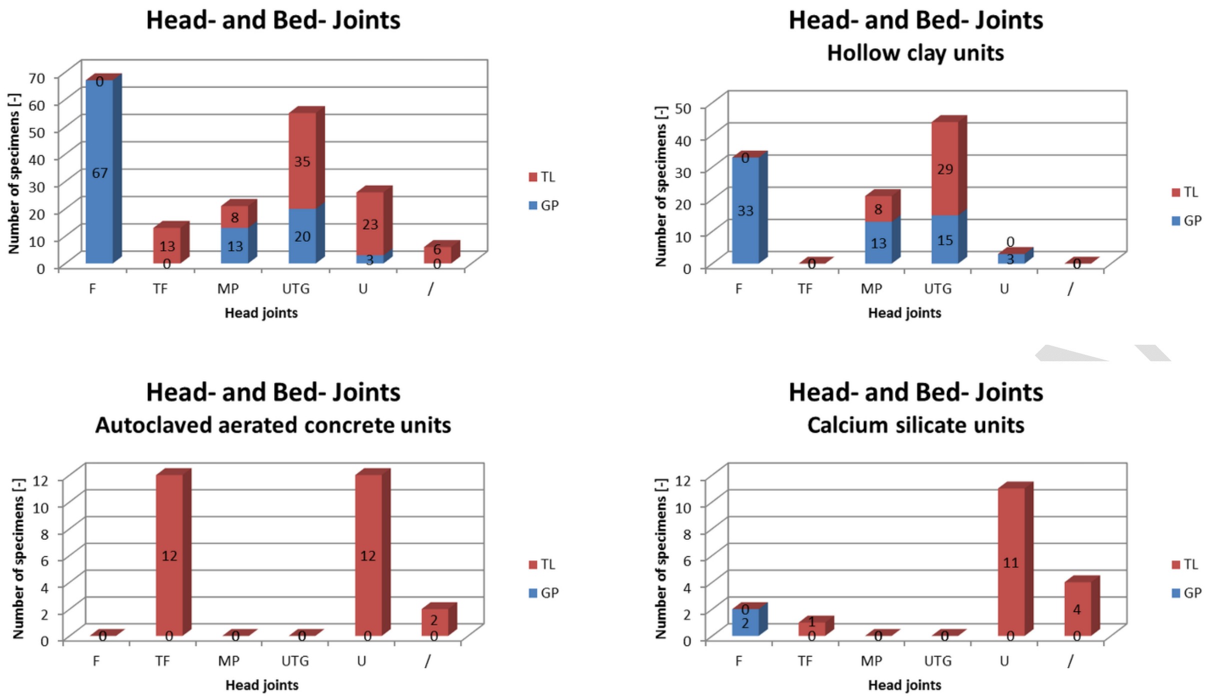

Figure 4. Head- and bed-joint typologies for some different masonry specimens.

2.3 Information on masonry walls

The third section contains eleven columns, reporting the main information about the masonry piers subjected to testing, in terms of both geometrical data of the wall and mechanical properties of the masonry. The first three columns (#1, #2, #3) report length (*l*), thickness (*t*) and height (*h*) of each tested masonry piers. Only tests on walls with height larger than 1.15 m have been included in the dataset. The in-plane wall slenderness (*h/l*) is calculated (#4) and the number of the masonry courses is also reported (#5). Figure 5 illustrates the number of the specimens at given intervals of piers' heights (from 1.17 m to 3.00 m). More than 20 walls are characterized by heights lower or equal to 1.50 m (10 less or equal to 1.25 m), being the majority included in the interval between 2.25 and 2.50 m. The number unit layers (masonry courses) goes from 5 to 46, being the larger values found for solid brick masonry.

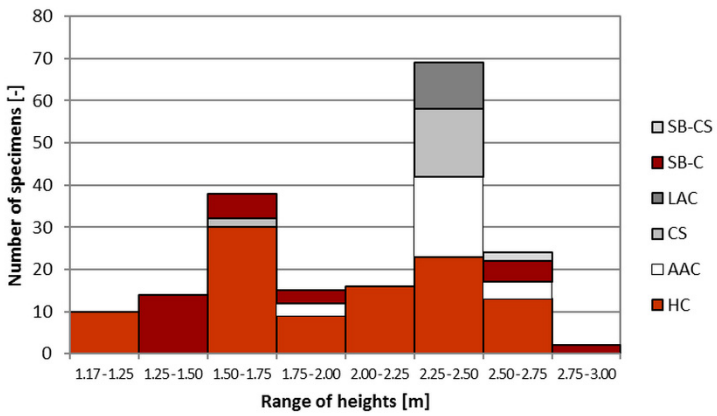

Figure 5. Number of specimens at given piers' height intervals ($x_{inf} < x \leq x_{sup}$).

The following columns include the values of the mechanical properties of the masonry typologies, including the experimental mean values of the strength and stiffness parameters, if available. In particular, the values of the vertical compression strength *f* (#8) and the elastic modulus *E* (#7), obtained from vertical compression tests on wallets, the values of diagonal tensile strength f_t (#11) and shear modulus *G* (#6), deducted from diagonal compression tests, and the values of the initial shear strength f_{v0} and friction coefficient μ of the mortar bed-joints (#9, #10), derived from shear tests on triplets, are reported. If no experimental data are available, for the evaluation of *f* and f_{v0}, the corresponding values have been calculated using the expressions and tables proposed in Eurocode 6 (EN 1996-1-1 [38]) and considering the conversion between the characteristic and the mean values through the relations $f=f_k \cdot 1.2$ and $f_{v0}=f_{vk0}/0.8$, according to EN 1052-1 [39] and EN 1052-3 [40] respectively; in the dataset, the so calculated values are reported in grey.

2.4 Test conditions

The fourth section contains four columns and reports the main information about the test conditions adopted for each specimen. The first two columns indicate the static scheme of the test, distinguishing between a "double-fixed" (no rotation of the top beam, "DF"), a cantilever (free rotation of the top beam, "C") and intermediate/other boundary conditions ("O") (#1), along with the corresponding h_0/h ratio (#2), where h_0 is the shear span (distance of the critical section from the zero moment one), equal to the height *h* of the wall for a "cantilever" condition and equal to $0.5 \cdot h$ for a wall "fixed" at both ends. As reported in Figure 6, the majority of the tests are conducted with "Cantilever" and "Double Fixed" boundary conditions, with exception of 6 specimens which are performed with intermediate conditions (5 in EPFL [14] and 1 at the University of Dortmund [10]).

The following two columns report the compression stress on the horizontal cross section of the wall σ_v (#3) resulting from the applied vertical load and the ratio σ_v/f between the compression stress and strength of the masonry (#4). Figure 7 reports the number of the specimens at given ranges of σ_v/f, showing that these ratios go from 2% to 41%, with the majority included between 2.5% and 22.5%.

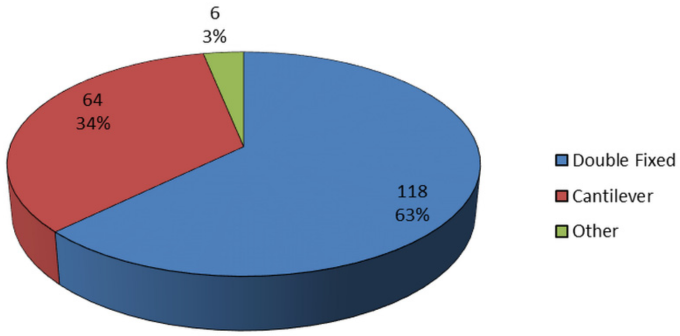

Figure 6. Composition of the dataset in terms of test boundary conditions.

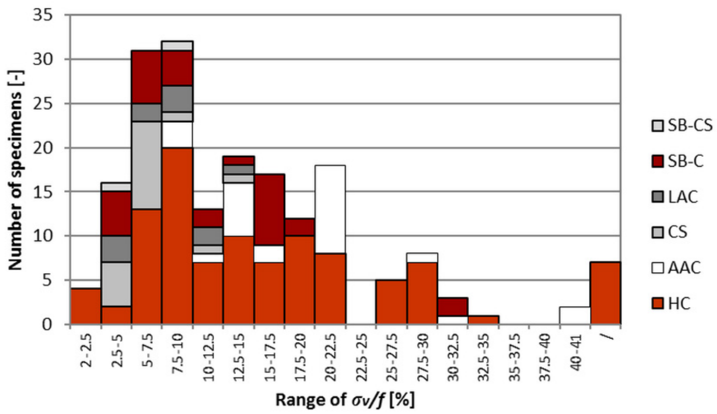

Figure 7. Number of the specimens at given intervals of σ_v/f ($x_{inf} < x \leq x_{sup}$); "\" indicates the cases when no compression strength was provided or evaluated.

2.5 Calculated lateral resistance

The fifth section contains twelve columns, with the calculation of the shear resistance of the specimens, starting from their geometrical and mechanical properties and according to the different code formulations proposed in the European seismic codes.

The resistant bending moment M_u of unreinforced masonry walls has been evaluated as in equation (1), included in the Italian norms for constructions (NTC 2018 [41]); the masonry wall is assumed subjected to longitudinally eccentric compression, with a rectangular stress diagram ("stress block") having a value of ultimate compression equal to $0.85 \cdot f_d$:

$$M_u = \frac{l^2 \cdot t \cdot \sigma_v}{2} \cdot \left(1 - \frac{\sigma_v}{0.85 \cdot f_d}\right) \tag{1}$$

where l is the length, t is the thickness of the wall, σ_v is the mean compression stress on the section of the panel ($\sigma_v = N/(l \cdot t)$, N is the vertical load) and f_d is the vertical compression strength of the masonry, taken as the mean value of the vertical compression strength. The lateral strength V_{flex} corresponding to flexural failure has been then calculated as M_u/h_0.

Regarding the shear failure, the corresponding lateral strength was calculated as the minimum value between V_{shear} and $V_{shear,lim}$ evaluated with the following expressions (equations (2) to (7)) derived from Eurocode 6 (EN 1996-1-1 [38]) and using the approach proposed by Magenes and Calvi [42] for the estimation of effective compressed uncracked section length l' under the hypotheses of neglecting the tensile strength of bed-joints and assuming a linear distribution of compression stresses:

$$V_{shear,i} = f_{vd} \cdot t \cdot l' \tag{2}$$

$$f_{vd} = f_{v0} + 0.4 \cdot \sigma_d \quad \text{for filled head-joints} \tag{3}$$

$$f_{vd} = 0.5 \cdot f_{v0} + 0.4 \cdot \sigma_d \quad \text{for unfilled head-joints} \tag{4}$$

$$V_{shear,lim,i} = f_{v,lim} \cdot t \cdot l' \tag{5}$$

$$f_{v,lim} = \frac{0.065}{0.8} \cdot f_b \quad \text{for filled head-joints} \tag{6}$$

$$f_{v,lim} = \frac{0.045}{0.8} \cdot f_b \quad \text{for unfilled head-joints} \tag{7}$$

where f_{vd} represents the shear strength of masonry, t is the thickness of the wall, f_{v0} is the mean value of the initial shear strength, σ_d is the mean compression stress on the portion of the wall subjected to compression ($\sigma_d = N/(t \cdot l')$, N is the vertical load) and f_b is the normalized vertical compression strength of the units. A coefficient equal to 1/0.8=1.25 has been applied to obtain a "mean" value of $f_{v,lim}$ from the characteristic value of $f_{vk,lim}$, in accordance with EN 1052-3 [40], that recommends a value of 0.8 between the mean and characteristic shear strength. Moreover, the expressions for the calculation of V_{shear} and $V_{shear,lim}$ have been limited to an upper bound ($V_{shear,max}$ and $V_{shear,lim,max}$) for the case of wall sections entirely subjected to compression ($l'=l$ and so $\sigma_d=\sigma_v$), whereas V_{shear} has also been limited to a lower value, $V_{shear,min}=0.4 \cdot N$, which corresponds to the minimum contribution of shear strength due to the masonry friction only. In the dataset, these latter values are indicated in grey if they are not exceeded.

The minimum value between V_{flex}, V_{shear} and $V_{shear,lim}$ represents the predicted lateral shear resistance of the walls (V_{pred}), and the lower value between the flexural and the shear strength provides the analytical identification of the failure mode that, therefore, could be by flexure ("*F*") or by shear ("*S*").

2.6 Experimental results from cyclic tests

The sixth section contains thirteen columns that summarize the most relevant experimental results of the in-plane cyclic tests.

Column #1 reports the failure mode identified for each test. From the available reports and papers, the failure modes obtained from the tests cover several cases, from flexural/rocking ("F") to pure shear ("S") with diagonal or step-wise cracking involving the joints and/or the units, "gaping" modes ("G") with stepped cracking mainly developed in the bed- and head-joints, sliding ("SL") at the ends of the walls. Additionally, on some tests, ambiguous or multi-failure modes have been often found, with the development of subsequent different failure modes; in this case, the mode was defined as hybrid ("H"). The failure modes in all the tests have been carefully re-checked, according to the damage pattern of the specimens found in the pictures of the documents, the type of hysteretic curves and the values of the maximum attained displacement; sometimes, this interpretation has led to change the original evaluation of the mechanisms stated in the available reports and papers, in particular for the case of the "hybrid" mechanisms, where the main involved modes have been always explicitly specified (for example, "H-FS" defines an hybrid mode with the occurrence of flexural and shear mechanisms). Finally, if even after the re-interpretation of the tests uncertainties or doubts in the detection of the failure mechanism were still found, "D", as doubtful, is indicated.

The following column (#2) contains an automatically coloured cell, green if the expected failure mode according to the code formulations is confirmed by the experimental results and red if not. If the experimental test has provided a "hybrid" mode involving one of the predicted modes (namely, shear or flexure), the cell is yellow if the analytical estimation is for shear, otherwise it is orange if the estimation is for flexure.

Column #3 reports the results of a classification of the tests in terms of equivalent viscous hysteretic damping ξ, calculated from the cyclic curves with the following expression based on the Jacobsen approach [43]:

$$\xi = \frac{W_d}{2 \cdot \pi \cdot (W_e^+ + W_e^-)} \tag{8}$$

where, for each complete cycle, W_d is the energy dissipated and $W_e^{+/-}$ is the elastic energy at peak displacement (see Figure 8).

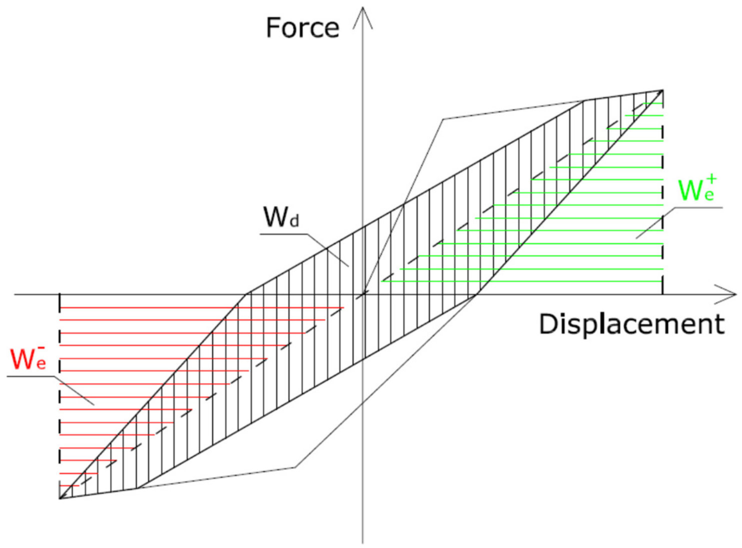

Figure 8. Definition of the parameters for the evaluation of the equivalent viscous damping.

A possible classification is indicated in equation (9). It is important to point out that this parameter has been evaluated and reported only for those experimental campaigns where the energy dissipation capacity has been processed. This classification should be considered as a qualitative measure that represents the general trend of energy dissipation beyond the cracking phase (i.e. inelastic behaviour). First and last cycles or not completed ones were not taken into account.

$$\xi \; range = \begin{cases} 1 & if \; \xi \leq 5\% \\ 2 & if \; 5\% < \xi \leq 15\% \\ 3 & if \; 15\% < \xi \leq 35\% \\ 4 & if \; \xi > 35\% \end{cases} \tag{9}$$

Column #4 reports the displacement at first visible crack in the specimen δ_{cr}. This information has been rarely found in the reports, also due to the difficulties in the identification of the first crack during a test.

The following three columns (#5, #6, #7) report the peak lateral force $V_{max,exp}$ obtained during the test, distinguished for positive ($^+$) and negative ($^-$) direction, and the ratio $V_{pred}/V_{max,exp}$ between the predicted shear (minimum value obtained from the code formulations) and the maximum experimental lateral force (maximum between positive and negative direction).

The displacements corresponding to the peak force in both directions $\delta_{Vmax,exp}{}^{+/-}$ are then indicated, followed by the positive and negative maximum displacements of the last fully completed cycles $\delta_{max,f}{}^{+/-}$ (after two or three cycles, depending by the loading history) and by the maximum displacements attained in the test in both directions $\delta_{max}{}^{+/-}$, independently by the full completion of all the cycles. It is worth noting that the values of $\delta_{max}{}^{+/-}$ do not necessarily correspond to collapse conditions (lacking of structural integrity and of the residual load-bearing capacity) since, in several cases, the tests have been stopped at a level of deformation that guaranteed a sufficient margin against collapse to preserve the instrumentation and maintain the safety laboratory requirements.

2.7 Parameters of the bilinear curves

A common approach to interpret the in-plane experimental response of masonry walls and to evaluate the related seismic parameters is to idealize the cyclic envelope of the hysteresis loops by means of a bilinear curve. For all the tests, the approach described in Frumento et al. [16] (hereafter reported for clearness) was consistently adopted and the obtained parameters are included in the seventh section of the dataset.

The first step for the evaluation of the bilinear curve is the construction of a cyclic envelope of the hysteresis loops, considering both positive and negative loading cycles, in order to evaluate the maximum lateral force and its degradation. Subsequently, the elastic stiffness $k_{el}^{+/-}$ is obtained by drawing the secant to the experimental envelope at $0.70 \cdot V_{max,exp}^{+/-}$, where $V_{max,exp}^{+/-}$ is the maximum force of the envelope curve in positive and negative direction. The displacement $\delta_u^{+/-}$ of the envelope curve is evaluated as the displacement corresponding to a strength degradation equal to 20% of $V_{max,exp}^{+/-}$. The value of the force $V_u^{+/-}$, corresponding to the horizontal branch of the bilinear curve, has been found by ensuring that the areas below the cyclic envelope curve and below the equivalent bilinear curve are equal. Knowing the elastic stiffness $k_{el}^{+/-}$ and the value of $V_u^{+/-}$, it was possible to evaluate the elastic displacement $\delta_e^{+/-}$, as $V_u^{+/-}/k_{el}^{+/-}$. The ductility is defined as $\mu_u^{+/-}=\delta_u^{+/-}/\delta_e^{+/-}$. The adopted definition of the parameters of the bilinear curve is given in Figure 9. However, since two or three loading-unloading cycles were carried out during the cyclic tests and two/three positive and negative envelopes and bilinear curves are obtained, a common procedure that allows to get only one positive and one negative bilinear curve for each tested wall has been implemented. The displacements $\delta_u^{+/-}$ are assumed as the lowest of the displacements of the three (or two) positive and of three (or two) negative cycles, respectively, whereas, the elastic displacements $\delta_e^{+/-}$ are instead assumed as the mean values of the positive and negative cycles, respectively. The ductility values $\mu_u^{+/-}$ are then computed as the ratios between $\delta_u^{+/-}$ and $\delta_e^{+/-}$, while μ_u is the minimum between the positive and negative ductility values. The equivalent values of $V_u^{+/-}$ have been assumed as the mean values of the V_u for each of the positive and negative cycles and the values of the equivalent elastic stiffness are therefore computed as $k_{el}^{+/-} = V_u^{+/-} / \delta_e^{+/-}$. It is finally important to point out that specimens did not reach a strength degradation of 20% of $V_{max,exp}$ in some of the performed tests, therefore in these cases, δ_u is assumed equal to the maximum displacement reached at the end of the test.

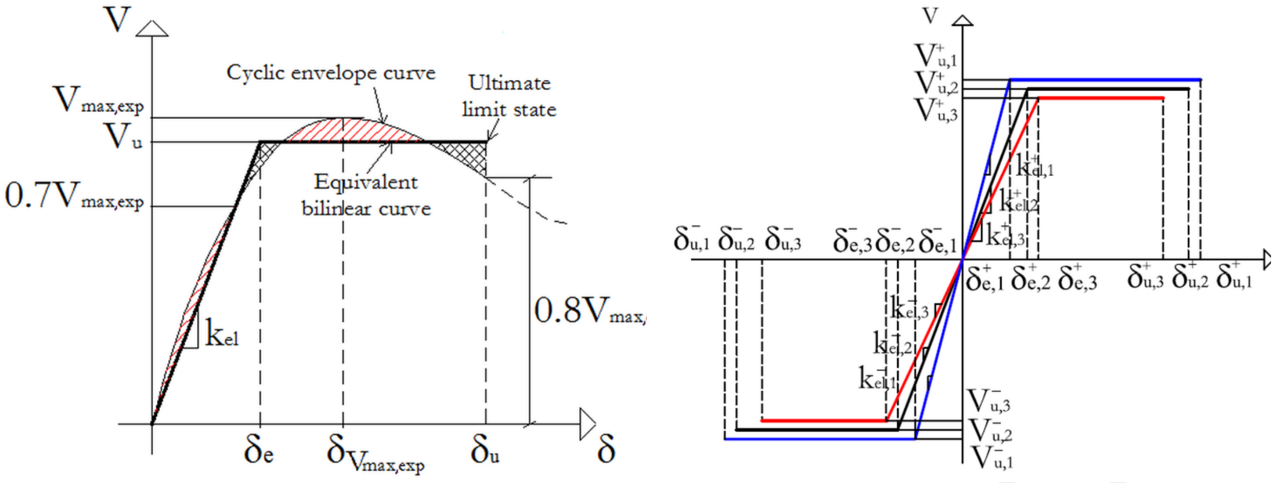

Figure 9. Idealization of the cyclic response: evaluation of the bi-linear curve from the hysteresis envelope.

2.8 Drift capacities

The eighth section contains six columns that summarize the main drift capacities identified for each specimen. The drift values are calculated dividing the horizontal displacements δ obtained from the tests by the height h of the specimens. With the exception of the drift at first crack θ_{cr}, the other drift values (at the elastic limit θ_e, at peak force θ_{Vmax}, at 0.8 times the peak force θ_u, at the maximum displacement of the last fully completed cycle $\theta_{max,f}$, and at the maximum displacement θ_{max}) are estimated taking the minimum displacement between the positive and the negative direction.

2.9 Example of the evaluation of the main parameters from cyclic tests and of the dataset layout

In Figure 10, an example of the evaluation of the main seismic parameters on the specimen “MA3” (research project [17]), is reported. The specimen “MA3” is a pier having length l=1.25 m and height h=2 m, made of a 35 cm thick masonry constituted by hollow clay units and bed- and head-joints filled by general purpose mortar; the test was carried out with “double fixed” boundary conditions and with a level of applied vertical mean compression stress σ_V=1.0 MPa. The envelope of the hysteretic curve is indicated with a bold black line, the construction of the bilinear curves with a red line.

In addition, in Table 4 an extract of the dataset of specimen “MA3” is also reported.

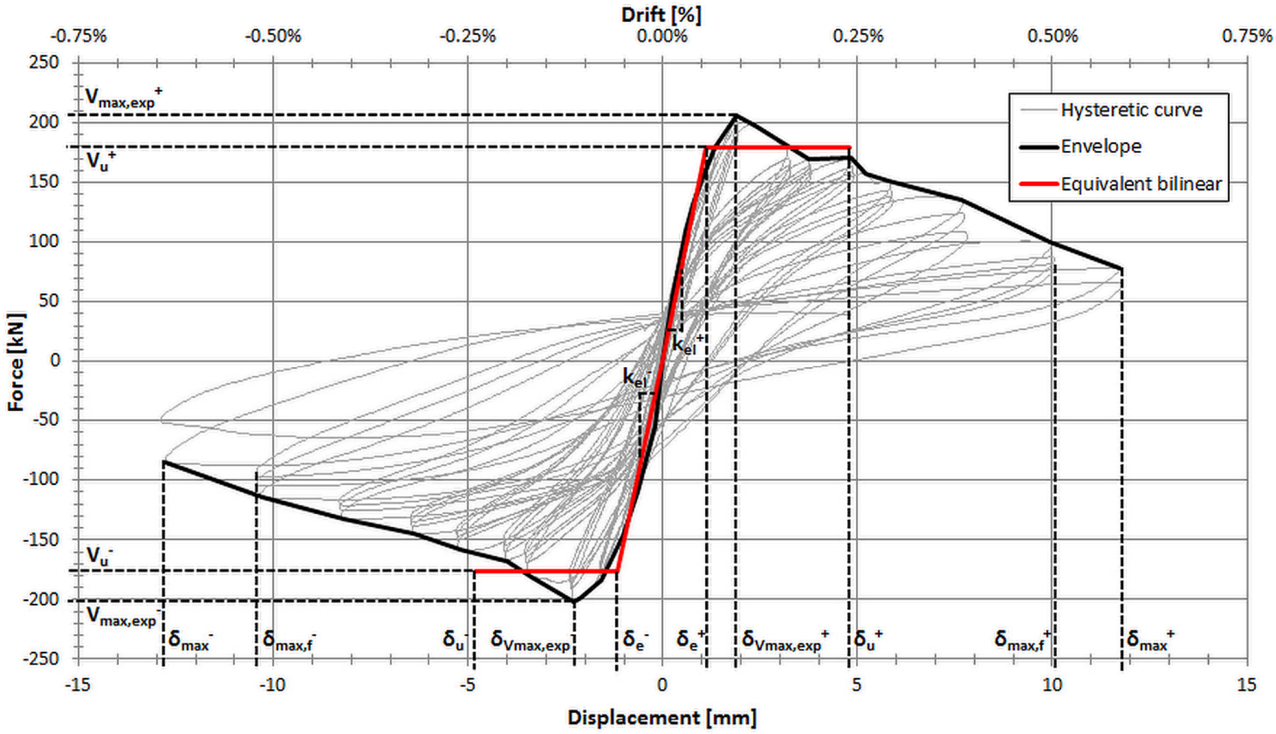

Figure 10. Example of the evaluation of the main parameters on the specimen “MA3” (research project [17]).

Table 4. Example of the dataset layout of specimen “MA3”.

	General Information and Reference [I]	
	#1	#2
N	Source	Specimen
139	*EUCENTRE [17]*	*MA3*

Information on Masonry Type, Units and Mortars [II]												
#1	#2	#3	#4	#5	#6	#7	#8	#9	#10	#11	#12	#13
Material	l_u [mm]	w_u [mm]	h_u [mm]	Void Ratio [%]	Unit density [kg/m^3]	f_b [MPa]	d [-]	$f_{b,norm}$ [MPa]	Bed Joints	Head Joints	Strength class	f_m [MPa]
HC	245	344	188	45%	1000	19.2	1.064	20.0	GP	F	M10	5.0

Information on Masonry Walls [III]										
#1	#2	#3	#4	#5	#6	#7	#8	#9	#10	#11
l [m]	t [m]	h [m]	h/l [-]	n° layers	G [MPa]	E [MPa]	f [MPa]	f_{v0} [MPa]	μ [-]	f_t [MPa]
1.25	0.350	2.00	1.60	10	1851	10800	9.50	0.69	0.77	0.41

Test conditions [IV]			
#1	#2	#3	#4
Boundary condition	ho/h [-]	σ_v [MPa]	σ_v/f [-]
DF	0.5	1.00	0.11

Calculated Resistances [V]											
#1	#2	#3	#4	#5	#6	#7	#8	#9	#10	#11	#12
M_u [kNm]	$f_{v,lim}$ [MPa]	V_{flex} [kN]	$V_{shear,i}$ [kN]	$V_{shear,min}$ [kN]	$V_{shear,max}$ [kN]	V_{shear} [kN]	$V_{shear,lim,i}$ [kN]	$V_{shear,lim,max}$ [kN]	$V_{shear,lim}$ [kN]	V_{pred} [kN]	Expected failure
239.6	1.63	239.6	236.4	175.0	476.9	236.4	217.6	710.9	217.6	217.6	S

Experimental Results (Cyclic Tests) [VI]												
#1	#2	#3	#4	#5	#6	#7	#8	#9	#10	#11	#12	#13
Failure mode	↓	ξ range	δ_{cr} [mm]	$V_{max,exp}^{+}$ [kN]	$V_{max,exp}^{-}$ [kN]	$V_{pred}/V_{max,exp}$	$\delta_{Vmax,exp}^{+}$ [mm]	$\delta_{Vmax,exp}^{-}$ [mm]	$\delta_{max,f}^{+}$ [mm]	$\delta_{max,f}^{-}$ [mm]	δ_{max}^{+} [mm]	δ_{max}^{-} [mm]
S	OK	3	/	206.5	201.6	1.05	1.89	2.30	10.07	10.41	11.80	12.90

Parameters Bilinear Curves [VII]										
#1	#2	#3	#4	#5	#6	#7	#8	#9	#10	#11
k_{el}^{+} [kN/mm]	k_{el}^{-} [kN/mm]	V_u^{+} [kN]	V_u^{-} [kN]	δ_e^{+} [mm]	δ_e^{-} [mm]	δ_u^{+} [mm]	δ_u^{-} [mm]	μ_u^{+}	μ_u^{-}	μ
159.6	149.2	178.8	176.0	1.12	1.18	4.78	4.83	4.3	4.1	4.1

Drift Capacities [VIII]					
#1	#2	#3	#4	#5	#6
Θ_{cr} [%]	Θ_e [%]	Θ_{Vmax} [%]	Θ_u [%]	$\Theta_{max,f}$ [%]	Θ_{max} [%]
/	0.056	0.095	0.239	0.504	0.590

3. LATERAL STRENGTH AND FAILURE MODES OF THE WALLS

Wall specimens with very few courses of masonry units and very low heights can be subjected to the issue of a "size effect", due to the higher influence of the boundary conditions, namely the confinement provided by the top and the bottom reinforced concrete or steel spreader beams, that can condition the results of the cyclic tests, in terms of lateral strength, effective failure modes and displacement capacity. In order to exclude this uncertain effect, specimens with heights *h* larger or equal to 1.50 m and more than 7 courses have only been considered in the following results. The sample has been consequently limited to 135 piers (62 hollow clay, 26 aerated autoclaved concrete, 18 calcium silicate, 11 lightweight aggregate, 16 solid clay brick and 2 calcium-silicate solid brick masonry), out of the 188 of the original dataset.

3.1. Values of lateral strength: correlation between test results and code expressions

Figure 11(a) and Figure 11(b) show a comparison between the values of the experimentally measured lateral resistance and the strength predicted by the codified expressions reported in paragraph 2.5, with the indication of the main experimental failure mechanisms. Furthermore, Figure 12(a) and Figure 12(b) represent the number/percentage of the specimens with different levels of accuracy between the predicted and the experimental strength, the former for all the specimens, the latter subdivided as a function of the effective experimental failure modes. Table 5 reports the intervals for the estimation of the accuracy levels in terms of ratio α between the predicted and the experimental values ($V_{pred}/V_{max,exp}$). Figure 11 and Figure 12 do not display the four tests with an uncertain failure mode and, obviously, the one for which the calculation of the lateral strength was not possible.

Table 5. Definition of accuracy levels

	$\alpha = V_{pred}/V_{max,exp}$
Good	$0.80 \leq \alpha \leq 1.10$
Intermediate	$0.70 \leq \alpha < 0.80$ & $1.10 < \alpha \leq 1.20$
Poor (conservative)	$\alpha < 0.70$
Poor (unconservative)	$\alpha > 1.20$

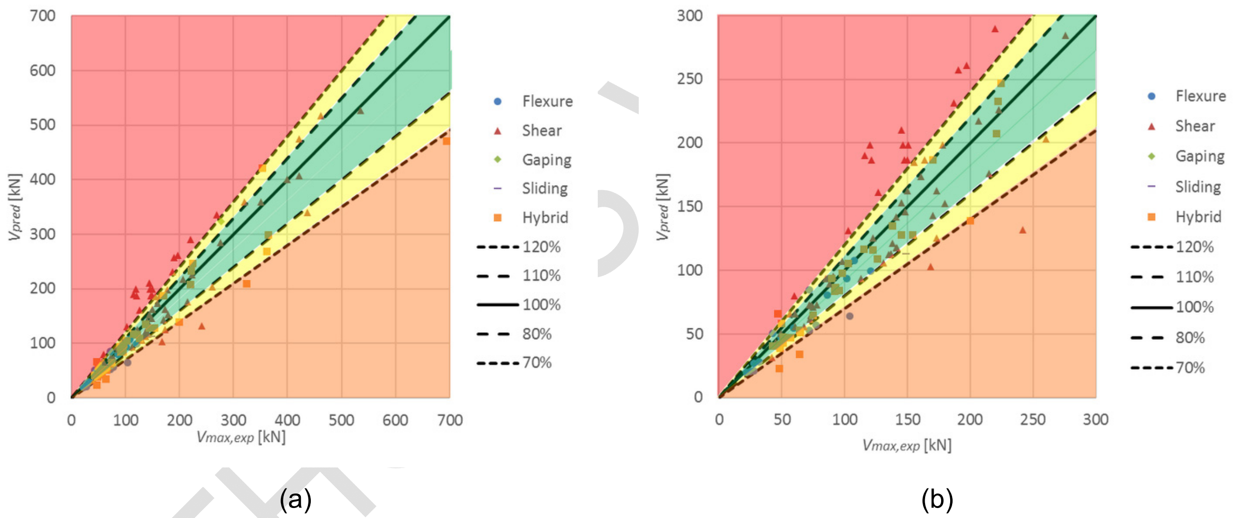

Figure 11. Correlation between experimentally measured and predicted strength by codified criteria: (a) and zoom up to forces of 300 kN (b).

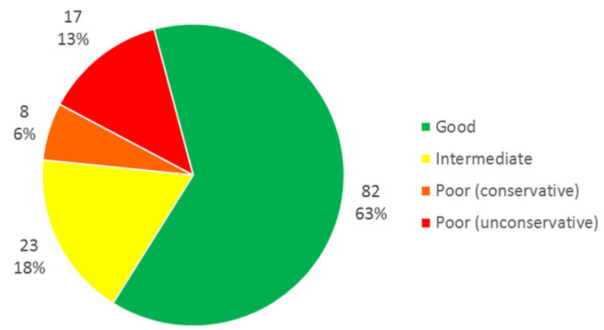

(a)

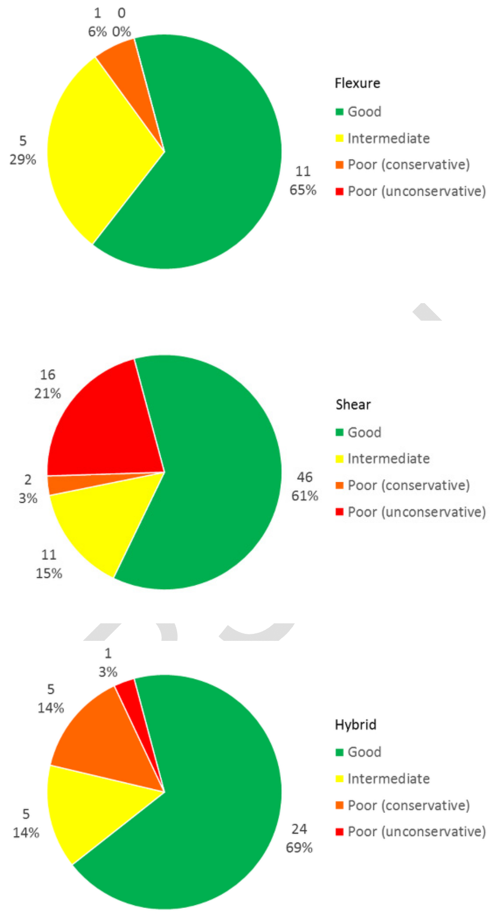

(b)

Figure 12. Number/percentage of specimens with different levels of $V_{pred}/V_{max,exp}$ for all the specimens (a) and as a function of the different experimental failure modes (b).

As inferable from Figure 12(a), good accuracy in the strength prediction is found for more than 60% of the specimens whereas, for 19% of the walls the ratio shows a poor prediction with a non-negligible over (6%) or under estimation (13%) of the lateral strength. As shown in the pie charts of Figure 12(b), the accuracy of the analytical strength prediction does not appear to be substantially influenced by the different effective failure modes although, in the case of flexural behaviour, the strength criterion based on ultimate moment matches test results with better precision than other modes and, in any case, often underestimating the actual resistance.

Finally, the test lateral resistance in the case of experimental shear failures have also been compared with the strength values derived by the Turnšek and Čačovič expression [44], calculated under the hypotheses formulated by Benedetti and Tomaževič [45] using the mean values of the diagonal tensile strength f_t (when available). As shown in the plots of Figure 13(a) and Figure 13(b), the formulation of EC6 fits better the experimental results in comparison with the Turnšek and Čačovič criterion, which tends in general to overestimate the lateral resistance of the piers with blocks. Given these results, only the EC6 expression for shear modes has been considered in the following investigations.

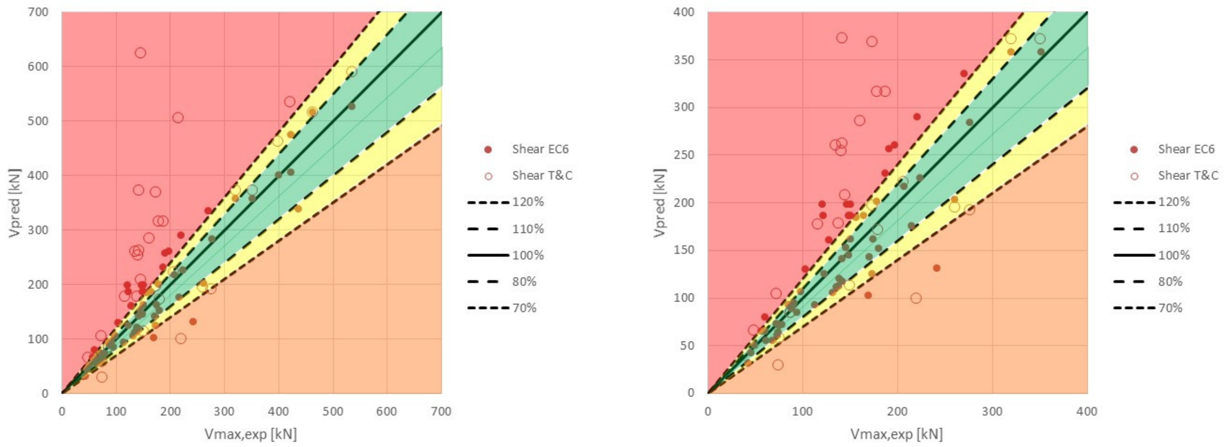

(a) (b)

Figure 13. Correlation between experimentally measured (only shear failure) and predicted shear strength by EC6 and Turnšek and Čačovič expressions (a) and zoom up to forces of 400 kN (b).

3.2. Identification of failure modes: correlation between test results and code criteria

Figure 14(a) illustrates the distribution of the failure modes derived from the interpretation of the experimental findings on the considered specimens, whereas Figure 14(b) shows the distribution of the predicted failure modes, by flexure or by shear, evaluated analytically as the lower value between the strength for flexure and the one for shear. Finally, Figure 15(a) and (b) report the scatter plot of the experimental and the predicted strength, where the green dots represent the situation when the expected failure mode according to the code formulations is confirmed by the experimental results, while the red triangles when it is not; if the experimental test has provided a “hybrid” mode involving the predicted estimated mode, the markers are light green if the analytical estimation is for shear, otherwise the markers are orange if the estimation is for flexure. Finally, Figure 16(a) and (b), report the number/percentage of specimens with different levels of accuracy in the analytical prediction of the experimental failure mechanisms, with the colours having the same meaning as above; the two pies of Figure 16(b) represent the failure mode prediction accuracy as a function of the flexural and shear estimated modes. Also Figure 15 and Figure 16 do not show the four tests with an uncertain failure mode and the test with the unknown value of lateral strength.

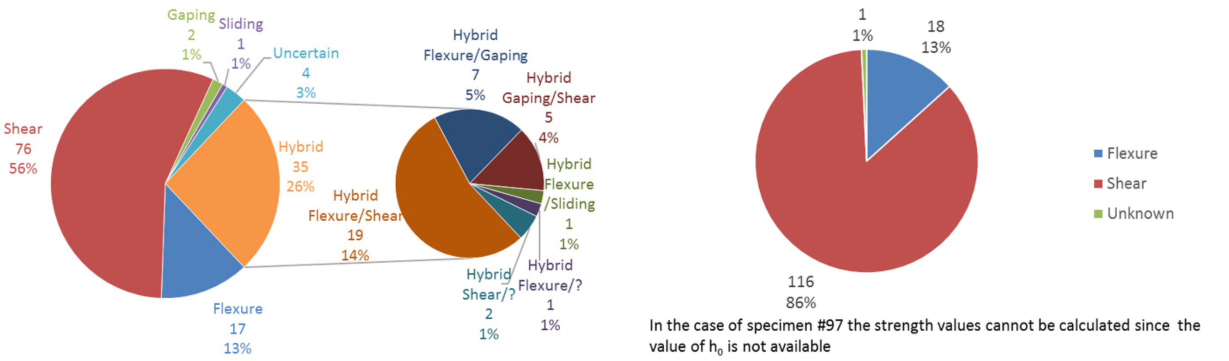

(a) (b)

Figure 14. Distribution of the experimental (a) and predicted (b) failure modes.

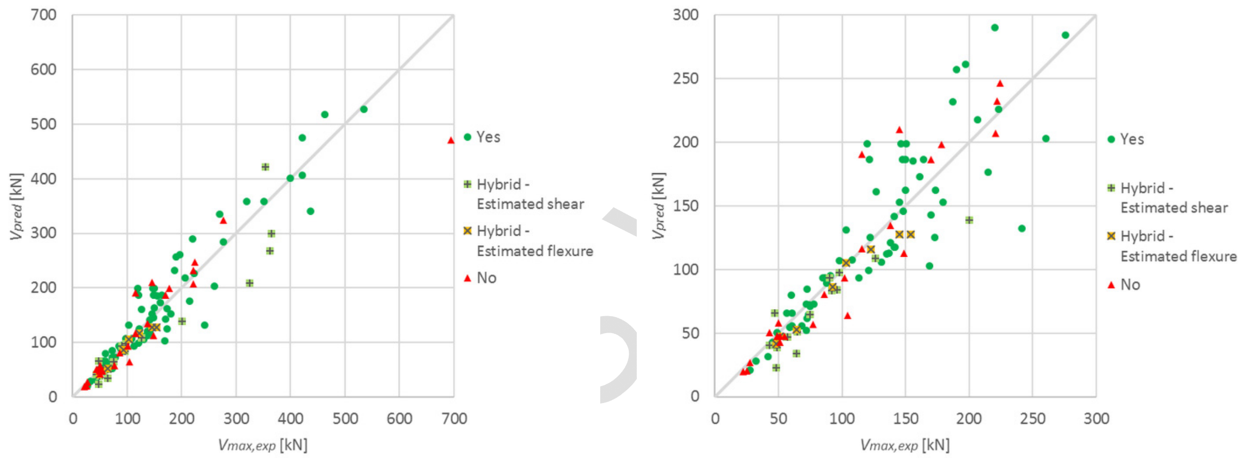

(a) (b)

Figure 15. Correlation between experimental and predicted strength in terms of accuracy of prediction of failure modes (a) zoom up to forces of 300 kN (b).

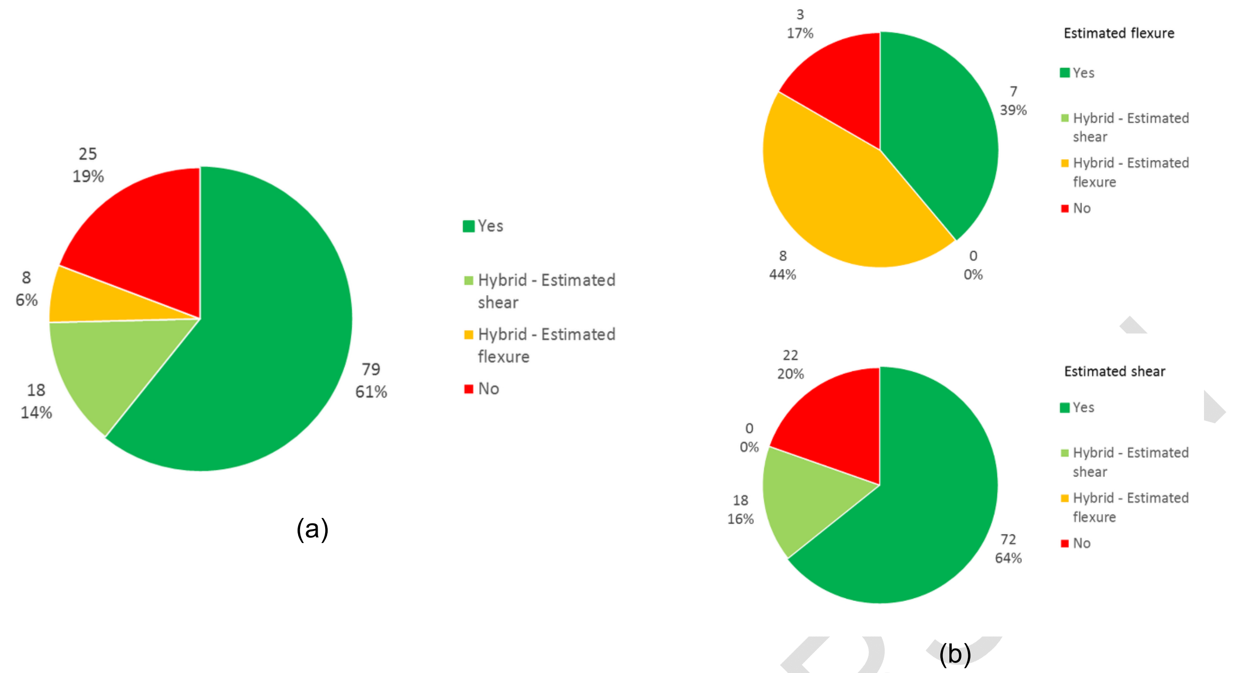

Figure 16. Number/percentage of specimens that match the failure modes for all the specimens (a) and as a function of the different estimated failure modes (b).

The accuracy in the prediction of the failure modes is not dependent by a good estimation of the lateral strength, as indicated in Figure 15(a) and (b) by the several red triangles lying close to the grey line representing the perfect match between the effective and the estimated resistance. Moreover, looking at Figure 16(a), the analytical estimation of the failure modes matches the effective experimental mechanisms for 61% of the specimens but, for almost 20% of the walls, the estimation is incorrect and increases up to 25% including the cases with “hybrid” modes involving also brittle mechanisms estimated as pure flexural. Besides, from the charts of Figure 16(b), it is evident that the failure prediction in the case of shear is more accurate than in the case of flexural modes, inferring that the expressions for the evaluation of the lateral strength for shear appear to be more safe-sided as respect to the one for flexure. In any case, a wrong prediction of the failure mode is present in almost 20% of the specimens, regardless the type of failure mechanisms.

4. DISPLACEMENT CAPACITY

Regarding the displacement capacity, the values of the experimental drift at peak force (θ_{Vmax}), the drift at 80% of V_{max} after the peak (θ_u) and at the maximum drift attained ($\theta_{max,f}$ and θ_{max}) are plotted in Figure 17 for all the tested specimens with the indication of the experimental failure mode.

In addition, in Figure 19, Figure 20 and Figure 21, these drift values have been divided in flexural/rocking, shear and hybrid failure mechanisms respectively, along with a summary of their statistical trends associated at each different masonry material. In these box and whiskers plots, minimum and maximum, mean and median, 25th and 75th percentile values and possible outliers have been represented with symbols specified in Figure 18. Figure 19 and Figure 20 also show the drift limits imposed in the previous Italian norms for constructions (NTC 2008 [46]), in the current ones (NTC 2018 [41]) and in part 3 of Eurocode 8 (EN 1998-3 [47]), as summarized in Table 6, in relation with the different failure modes (shear and flexure) and with the limit states (Damage Limitation “DL”, Severe Damage “SD” and Near Collapse “NC” Limit States). Table 7 finally reports the main statistical parameters of drift divided by failure modes and masonry material.

Table 6. Drift limits on URM piers in the considered European norms.

	Damage Limitation (DLLS) [%]	**Severe Damage (SDLS) [%]**		**Near Collapse (NCLS) [%]**	
	-	**Flexure**	**Shear**	**Flexure**	**Shear**
NTC 2008	0.3	0.8	0.4	-	-
NTC 2018	0.2	-	-	1.0	0.5
EC8-part 3	-	$0.8 \cdot h_0/l$	0.4	$1.07 \cdot h_0/l$	0.53

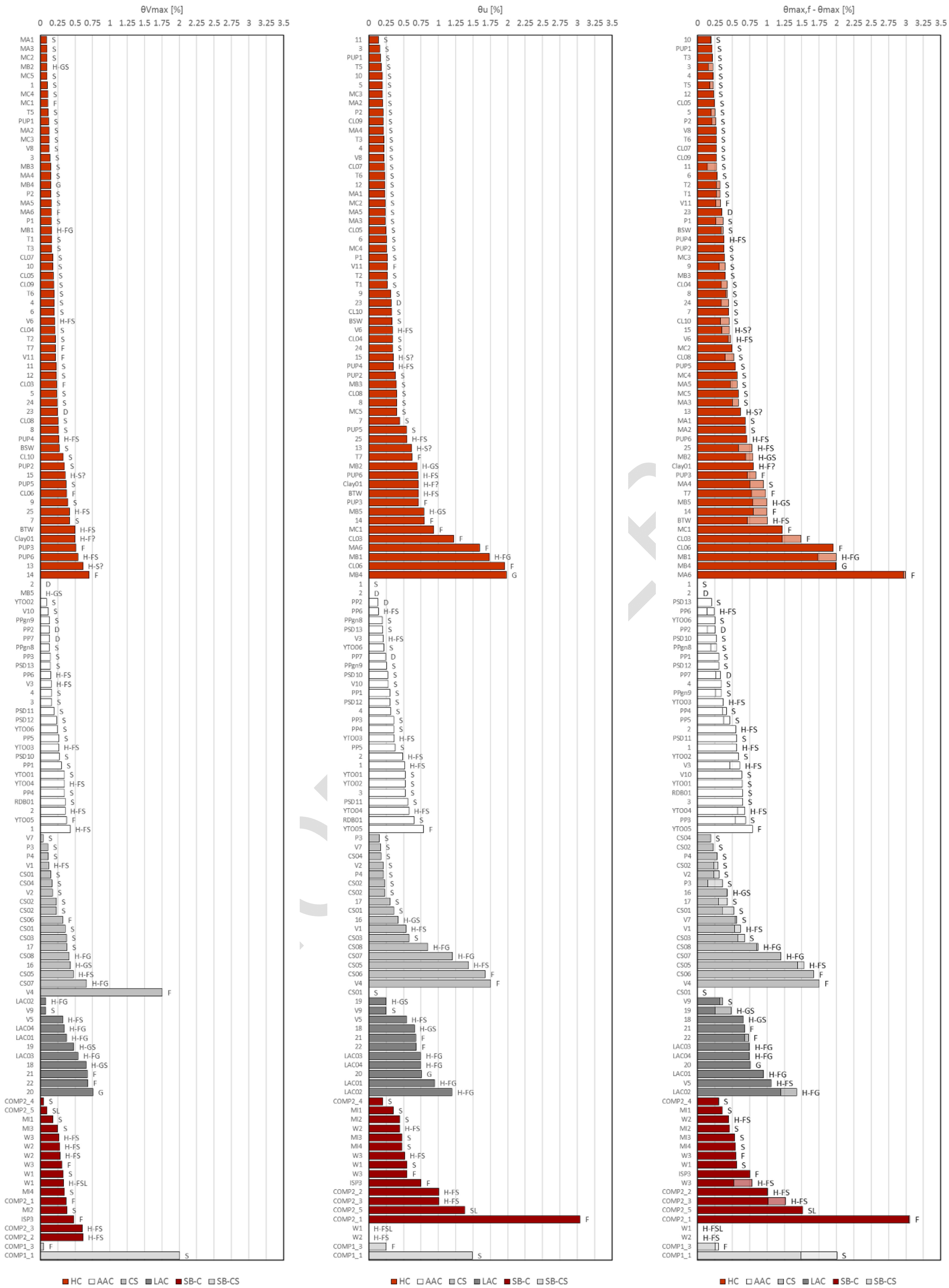

(a) (b) (c)

Figure 17. Experimental drift values: at peak force θ_{Vmax} (a), at 20%-drop of V_{max} (b), and at the maximum $\theta_{max,f}$ and θ_{max} (c).

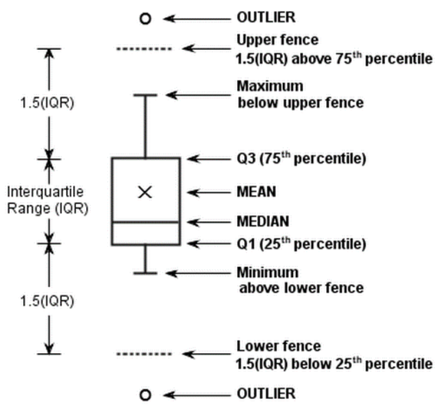

Figure 18. Definition of the statistical parameters associated with the drift values in box and whiskers plots.

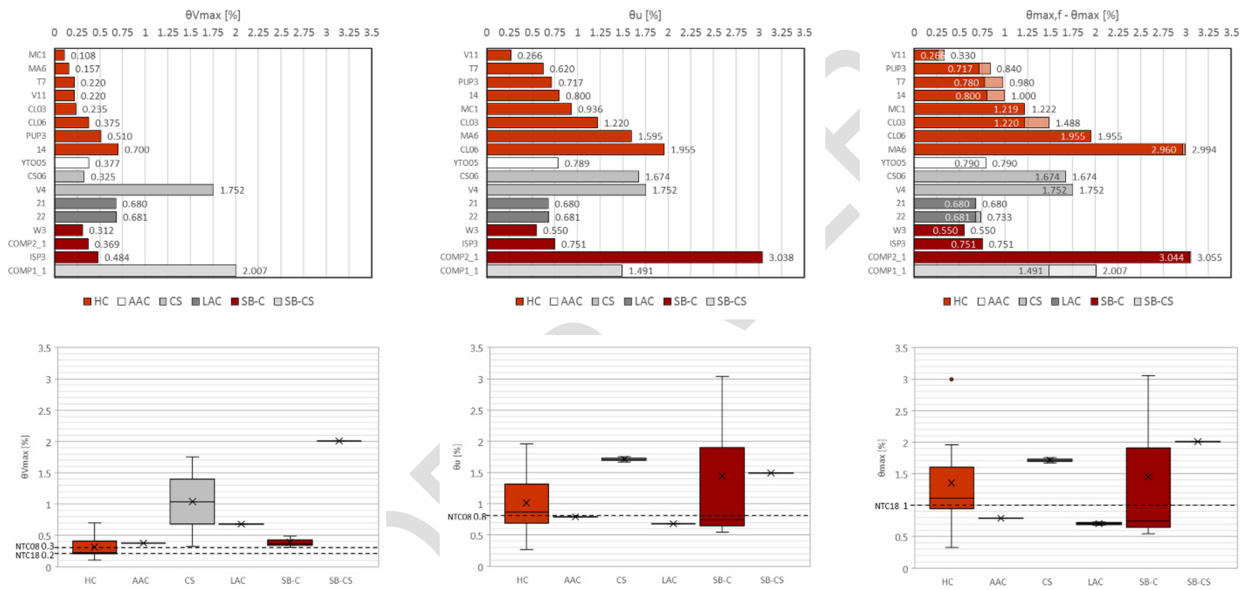

(a) (b) (c)

Figure 19. Experimental drift values for flexural/rocking mechanisms: at peak force θ_{Vmax} (a), at 80% of V_{max} after the peak θ_u (b), and at the maximum $\theta_{max,f}$ and θ_{max} (c) and corresponding box and whiskers plots for different masonry materials. The limits for EC8 are not reported.

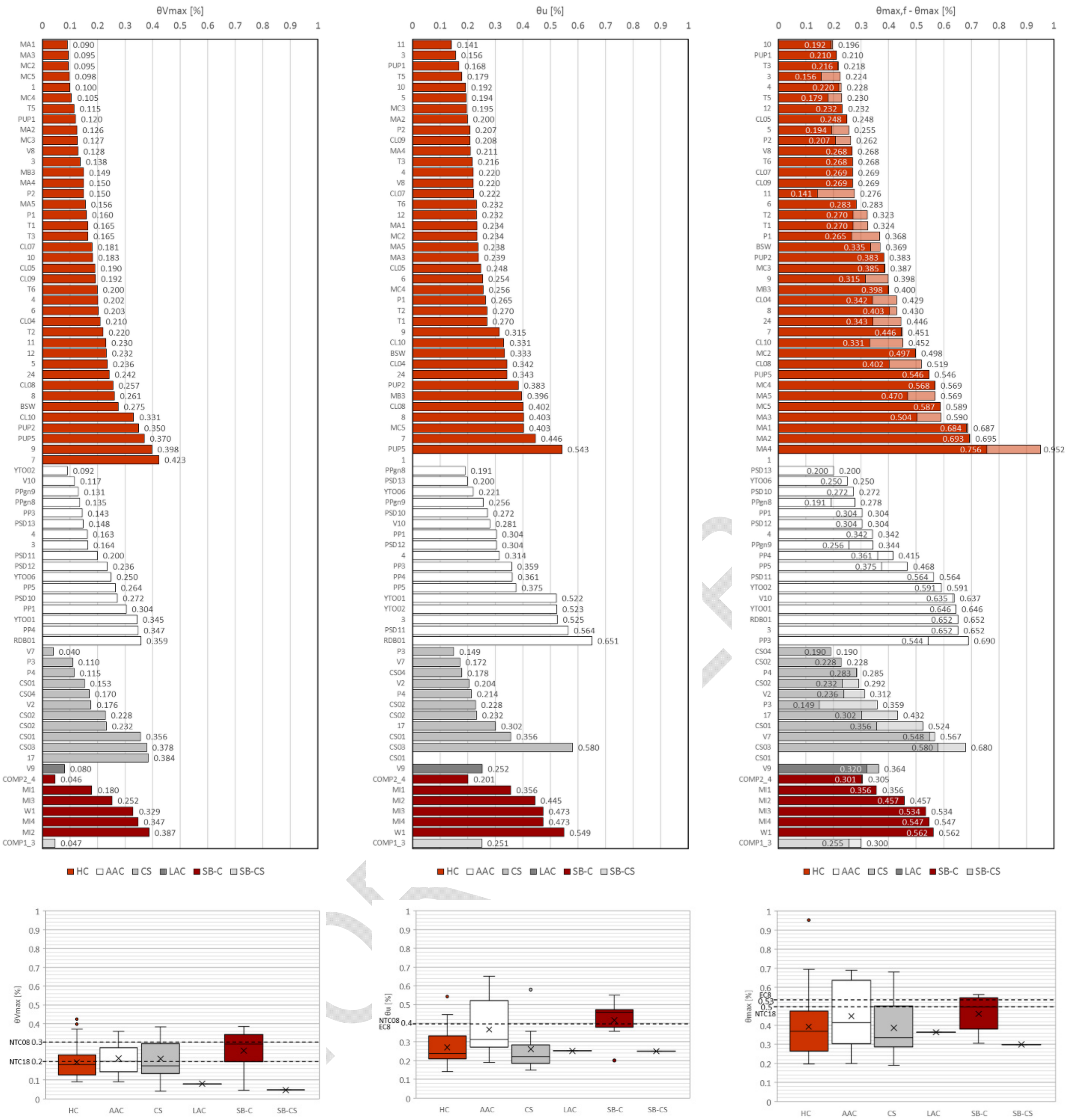

(a) (b) (c)

Figure 20. Experimental drift values for shear failures: at peak force θ_{Vmax} (a), at 80% of V_{max} after the peak θ_u (b), and at the maximum $\theta_{max,f}$ and θ_{max} (c) and corresponding box and whiskers plots for different masonry materials.

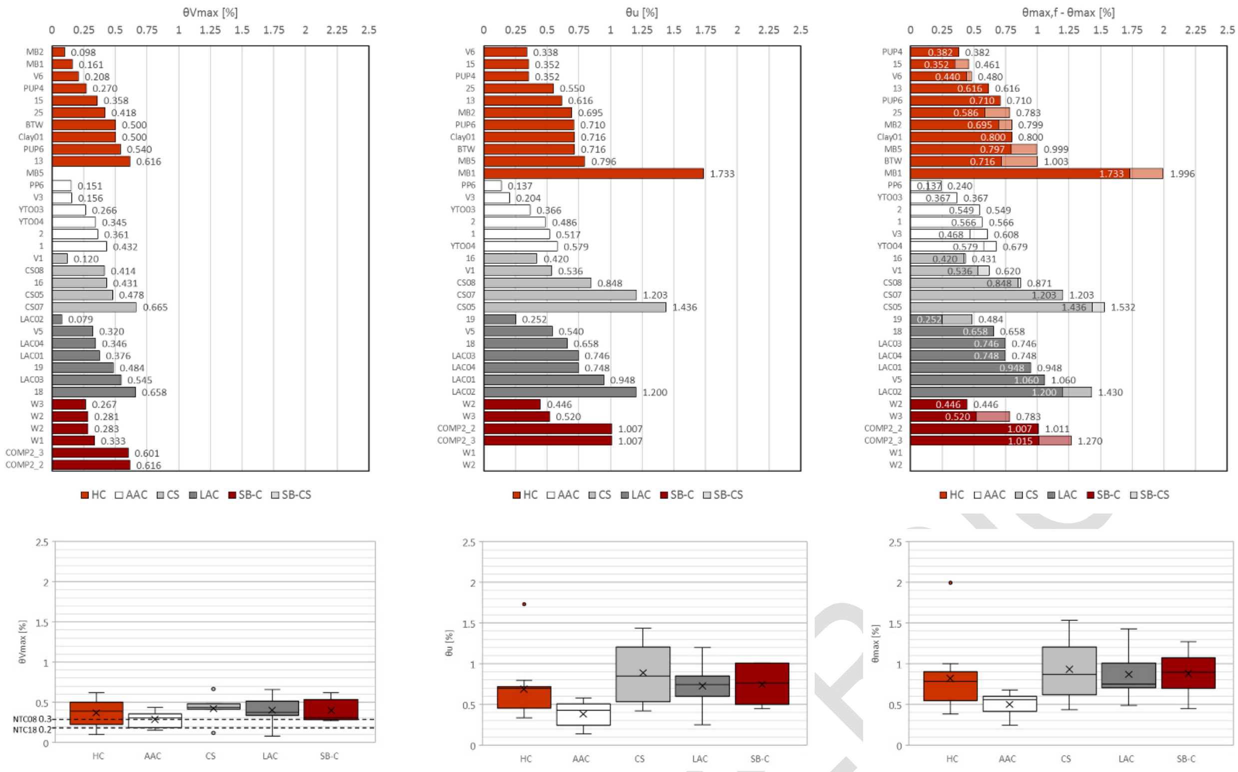

(a) (b) (c)

Figure 21. Experimental drift values for hybrid failures: at peak force θ_{Vmax} (a), at 80% of V_{max} after the peak θ_u (b), and at the maximum $\theta_{max,f}$ and θ_{max} (c) and corresponding box and whiskers plots for different masonry materials .

Table 7. Values of drifts associated with different failure mechanisms and divided by masonry material.

		FLEXURAL				SHEAR				HYBRID			
		θ_{Vmax} [%]	θ_u [%]	$\theta_{max,f}$ [%]	θ_{max} [%]	θ_{Vmax} [%]	θ_u [%]	$\theta_{max,f}$ [%]	θ_{max} [%]	θ_{Vmax} [%]	θ_u [%]	$\theta_{max,f}$ [%]	θ_{max} [%]
ALL	**mean**	0.56	1.15	1.25	1.34	0.20	0.30	0.37	0.41	0.37	0.68	0.71	0.80
	st. dev.	0.51	0.67	0.78	0.78	0.10	0.12	0.16	0.16	0.16	0.35	0.34	0.37
	median	0.38	0.80	0.80	1.00	0.18	0.26	0.33	0.37	0.36	0.62	0.66	0.75
	max	2.01	3.04	3.04	3.06	0.42	0.65	0.76	0.95	0.67	1.73	1.73	2.00
	min	0.11	0.27	0.27	0.33	0.04	0.14	0.14	0.19	0.08	0.14	0.14	0.24
HC	**mean**	0.32	1.01	1.24	1.35	0.20	0.27	0.35	0.39	0.37	0.69	0.71	0.82
	st. dev.	0.19	0.51	0.80	0.76	0.08	0.09	0.15	0.16	0.17	0.37	0.36	0.42
	median	0.23	0.87	1.01	1.11	0.18	0.24	0.32	0.37	0.39	0.69	0.69	0.78
	max	0.70	1.95	2.96	2.99	0.42	0.54	0.76	0.95	0.62	1.73	1.73	2.00
	min	0.11	0.27	0.27	0.33	0.09	0.14	0.14	0.20	0.10	0.34	0.35	0.38
AAC	**mean**	0.38	0.79	0.79	0.79	0.22	0.37	0.42	0.45	0.29	0.38	0.44	0.50
	st. dev.	0.00	0.00	0.00	0.00	0.09	0.14	0.17	0.17	0.10	0.16	0.16	0.15
	median	0.38	0.79	0.79	0.79	0.20	0.31	0.36	0.42	0.31	0.43	0.51	0.56
	max	0.38	0.79	0.79	0.79	0.36	0.65	0.65	0.69	0.43	0.58	0.58	0.68
	min	0.38	0.79	0.79	0.79	0.09	0.19	0.19	0.20	0.15	0.14	0.14	0.24
CS	**mean**	1.04	1.71	1.71	1.71	0.21	0.26	0.31	0.39	0.42	0.89	0.89	0.93
	st. dev.	0.71	0.04	0.04	0.04	0.11	0.12	0.14	0.15	0.18	0.39	0.39	0.40
	median	1.04	1.71	1.71	1.71	0.18	0.22	0.26	0.34	0.43	0.85	0.85	0.87
	max	1.75	1.75	1.75	1.75	0.38	0.58	0.58	0.68	0.67	1.44	1.44	1.53
	min	0.33	1.67	1.67	1.67	0.04	0.15	0.15	0.19	0.12	0.42	0.42	0.43
LAC	**mean**	0.68	0.68	0.68	0.71	0.08	0.25	0.32	0.36	0.40	0.73	0.80	0.87
	st. dev.	0.00	0.00	0.00	0.03	0.00	0.00	0.00	0.00	0.17	0.28	0.29	0.29
	median	0.68	0.68	0.68	0.71	0.08	0.25	0.32	0.36	0.38	0.75	0.75	0.75
	max	0.68	0.68	0.68	0.73	0.08	0.25	0.32	0.36	0.66	1.20	1.20	1.43
	min	0.68	0.68	0.68	0.68	0.08	0.25	0.32	0.36	0.08	0.25	0.25	0.48
SB-C	**mean**	0.39	1.45	1.45	1.45	0.26	0.42	0.46	0.46	0.40	0.75	0.75	0.88
	st. dev.	0.07	1.13	1.13	1.14	0.12	0.11	0.10	0.10	0.15	0.26	0.27	0.30
	median	0.37	0.75	0.75	0.75	0.29	0.46	0.50	0.50	0.31	0.76	0.76	0.90
	max	0.48	3.04	3.04	3.06	0.39	0.55	0.56	0.56	0.62	1.01	1.01	1.27
	min	0.31	0.55	0.55	0.55	0.05	0.20	0.30	0.31	0.27	0.45	0.45	0.45
SB-CS	**mean**	2.01	1.49	1.49	2.01	0.05	0.25	0.25	0.30	-	-	-	-
	st. dev.	0.00	0.00	0.00	0.00	0.00	0.00	0.00	0.00	-	-	-	-
	median	2.01	1.49	1.49	2.01	0.05	0.25	0.25	0.30	-	-	-	-
	max	2.01	1.49	1.49	2.01	0.05	0.25	0.25	0.30	-	-	-	-
	min	2.01	1.49	1.49	2.01	0.05	0.25	0.25	0.30	-	-	-	-

With the exception of two calcium-silicate specimens failing in pure flexure, the values of drift at peak force θ_{Vmax} have ranged in a rather limited interval between approximately 0.10% and 0.50% with a mean value of about 0.25%, independently by the masonry typologies and the final failure mode. These values of drift at peak force could be assumed as a reference value for the Damage Limitation Limit State (DLLS), as defined in Eurocode 8 [47] and in Italian codes ([46], [41]). NTC 2008 [46] limits the drift at DLLS for URM buildings to 0.30%, whereas NTC 2018 [41] to 0.20%. No explicit limitation at DLLS for structural masonry buildings is instead present in EC8 [47]. As observable in Figure 19(a), Figure 20(a) and Figure 21(a), the drift threshold at DLLS proposed in NTC 2018 [41] appears to be appropriate.

On the other side, the values of drift θ_u, which are commonly related to life preservation/severe damage, as defined in the previous Italian norms (NTC2008 [46]) for the Life Safety/Severe Damage Limit State (SDLS), differ significantly as a function of the different experimental failure modes and masonry material. In particular, for pure shear failures, drifts between about 0.15% and 0.60% have been obtained, with a minimum value of 0.14% for a specimen with hollow clay units. Mean values of θ_u of 0.30% have been found overall, 0.27% for hollow clay unit masonry, 0.37% for AAC masonry, 0.26% for calcium-silicate masonry, 0.25% for lightweight aggregate concrete masonry (on only one specimen failing in shear) and 0.42% for clay solid brick masonry. Conversely, walls characterized by flexural/rocking mechanisms have provided much higher values of drift θ_u, on average, overall larger than 1.10% and very few cases below 0.70%; in the case of hollowed clay unit masonry, the mean value is equal to about 1.0% (the median equal to 0.87%) whereas, for solid clay brick masonry, to about 1.45% with however a much lower median value, equal to 0.75%. For the other materials, few specimens have provided pure flexural mechanisms, in any case with values larger than about 0.70%. Specimens with hybrid modes have instead obtained intermediate values of drift θ_u between pure shear and hybrid failure modes. The overall mean value of drift is settled around 0.70% and it is almost equal for all the materials, with the exception of the AAC masonry that provides lower levels of deformation capacity (0.38%). The previous Italian norms (NTC 2008 [46]) limit the drift at SDLS for URM buildings to 0.40% in case of shear modes and to 0.80% for flexural modes, whereas the EC8-part 3 [47] to 0.40% and to $0.80 \cdot h_0/l$%, respectively. As evidenced by Figure 19(b) and Figure 20(b), the drift limits at SDLS proposed in the previous Italian norms [46] and in the EC8 [47] seem to be adequate for flexural modes but in general overestimate the displacement capacity in the case of shear failures.

Similarly, the values of maximum drift capacity achieved at the end of the test $\theta_{max,f}$ and θ_{max}, which could be conservatively related to the Near Collapse Limit State (NCLS) as defined in Eurocode 8 [47] and in the current Italian norms [41], differ significantly as a function of the masonry typologies and of the different failure modes. In the case of pure shear mechanisms, the overall mean values of θ_{max} is 0.41% (θ_u = 0.30%; θ_{max} = 0.39% for HC, 0.45% for AAC, 0.39% for CS, 0.36% for LAC, 0.46% for SB-C). The values of maximum drift for flexural modes is 1.35% for the hollow clay masonry, whereas it is approximately at the same level for solid clay brick masonry; even in this case, as for θ_u, a significant difference between the mean and the median values has been found. The overall mean of drift θ_{max} for hybrid modes is 0.80% (θ_u = 0.68%). For shear and hybrid modes, the difference between θ_{max} and $\theta_{max,f}$ is more significant than for the case of flexural modes; in the former case, the overall mean $\theta_{max,f}$ is 0.37% (θ_{max} = 0.41%) while, in the latter case, equal to 0.71% (θ_{max} = 0.80%). The most significant differences between the mean values of θ_{max} and $\theta_{max,f}$ are noticed for hollow clay unit and calcium-silicate masonry in the case of shear failures (θ_{max} = 0.39%, $\theta_{max,f}$ = 0.35% for HC and θ_{max} = 0.38%, $\theta_{max,f}$ = 0.31% for CS); no differences are present for clay brick masonry for shear modes. The current Italian norms [41] limit the drift at NCLS for URM buildings to 0.50% in case of shear modes and to 1.00% for flexural modes, whereas the EC8-part 3 [47] to 0.53% and to $1.07 \cdot h_0/l$ %, respectively. As for SDLS, the drift limits for NCLS recommended in the EC8 and in the current Italian norms provide adequate values for flexural modes but overestimate the displacement capacity in the case of shear failures, as shown in Figure 19(c) and Figure 20(c).

Finally, an investigation on possible bias in the statistical analyses of the results due to the execution of about 30% of the tests in the same laboratory (in Pavia) has been conducted, comparing the different parameters (i.e., lateral resistance and drift capacity) with and without the tests carried out in Pavia. The trends do not differ significantly, with the only exception of the ultimate and maximum drift capacity of piers with flexural modes, that were found to be lower excluding the tests in Pavia (the mean values of θ_u and θ_{max} decrease respectively from 1.15% to 0.75% and from 1.34% to 0.85%). This reduction may be ascribed to the application of lower compressive stress, in average, in the Pavia tests but also to the degree of subjectivity in defining ultimate conditions of the specimens (i.e., when a laboratory decides to stop the test). However, it appears important to consider all the processed results, because provide an essential contribution for some specific masonry typologies and improve the reliability of the whole dataset without modifying the general trends observed analysing the data of other laboratories.

5. CONCLUSIONS

A dataset that assembles the results of 188 in-plane cyclic tests carried out mainly in Europe on unreinforced masonry piers with bricks and blocks, having different materials and typologies, dimensions, boundary conditions, vertical applied loads and horizontal loading history, has been developed, along with the available results of tests of characterization on units, mortar and masonry. The dataset can be freely downloaded [35] and will be continuously updated following the same criteria. It is important to underline that in this work the largest effort was devoted to the preparation of the dataset itself, which is mainly intended to provide a tool available for future studies aiming at the improvement of the understanding of the in-plane response of URM walls. The aspects here discussed concerning the in-plane lateral strength and displacement capacity only represent a small and introductory part of what can be obtained with the use of these data. The framework of this dataset can also be used as reference on the minimum basic parameters needed for a correct execution and interpretation of in-plane cyclic tests, although additional information on units (e.g., geometrical configurations of hollow blocks, tensile strength, elastic modulus), mortar (e.g., composition, flexural and tensile strength, elastic modulus) and standards used in tests of characterization may be helpful. It is emphasized that some fundamental information, for example the density of the units, the modulus of elasticity (in particular the shear modulus G), the friction coefficient μ, the diagonal tensile strength f_t of masonry and the results of energy dissipation, was often missing. In some cases, even the values of compressive strength of units f_b, mortar f_m and masonry f and of shear strength of masonry f_{v0} were not available.

For the proposed preliminary interpretation of the test results, only specimens with heights $h \geq 1.50$ m and number of courses with more than 7 have been considered, in order to avoid possible "size effect" issues that can condition the results of the cyclic tests and influence a realistic evaluation of the lateral strength, of the effective failure modes and of the displacement capacity.

The lateral strength of the piers obtained from the experiments has been correlated with the expressions provided by Eurocode 6 [38] and by the current Italian norms for construction (NTC 2018 [41]) and the failure modes have been identified analytically and compared with the test results. The comparison between the experimental and the predicted lateral strength has provided a good accuracy for more than 60% of the specimens whereas, for 19% of the walls, the prediction is found to be poor with a quite significant over or under estimation of the lateral strength. Moreover, the analytical estimation of the failure modes has led to incorrect results in almost 20% of the specimens up to 25% including the cases with "hybrid" modes involving also brittle mechanisms estimated as pure flexural. The codified expressions do not consider the occurrence of other mechanisms unless pure shear or flexural and, therefore, in the case of other modes (e.g., gaping or hybrid), no correspondence between the analytical and the experimental estimation is possible. The application of the Turnšek and Čačovič criterion [44] on the specimens with shear failures has provided results which overestimate significantly the lateral shear resistance of the tested piers with blocks and suggest that this expression is more appropriate when applied on irregular masonry, like irregular and uncut stone masonry, as also mentioned by Vanin et al. [34] and in the instructions for the application of the NTC2008 [48].

Regarding the deformation capacity at the ultimate limit states ("Severe Damage" and "Near Collapse" Limit States), the results are found to be very scattered and to be mainly influenced by the type of failure modes, which depends in turn by the level of compression, and by the masonry typology (and, within the same typology, in relation with other characteristics such as the head-joint types). Although no systematic relationship has been provided between drift capacity and vertical stress, it is clear that the displacement capacity reduces for shear failure modes, which are usually activated for higher compressions. In the case of pure shear, an overall mean value of drift θ_u equal to 0.30% has been obtained, with results varying as a function of different masonry typologies (i.e., 0.27% for hollow clay unit masonry, 0.42% for clay solid brick masonry). Walls characterized by flexural/rocking mechanisms have instead provided much higher values of drift θ_u, being, on average, larger than 1.10%, whereas in the case of hybrid modes, intermediate values of drift θ_u between the case of pure shear and flexural failure modes have been found (overall mean drift equal to about 0.70%). Similarly, the values of maximum drift capacity achieved at the end of the test θ_{max} differ significantly as a function of the masonry typologies and of the different failure modes attaining, in the case of pure shear mechanisms, an overall mean value of θ_{max} of 0.41%, whereas for flexural and hybrid modes of 1.34% and 0.80%, respectively. The drift limits at ultimate limit states reported in the Italian norms ([46], [41]) and in Eurocode 8 part 3 [47] seem to be adequate for flexural modes but, in general, overestimate the displacement capacity in the case of shear failures. Finally, it is important to stress that the results of the drift capacity at ultimate conditions may be significantly affected by a degree of subjectivity (i.e., the moment a test is stopped) and it is suggested to keep on incrementing the lateral loading until actual near collapse conditions of the specimen are attained (i.e., significant loss of lateral resistance/reduced loadbearing capacity).

It is evident that these outcomes demonstrate the need of further investigation on the main seismic parameters that influence the in-plane response of unreinforced masonry walls. The current European norms clearly provide an evaluation of the lateral strength and on the deformation capacity of the piers which is not always consistent with the experimental findings and, sometimes, also unsafe, without any differentiation in relation with different materials (clay vs. lightweight concrete vs. AAC….) and, within a given material, with the types of blocks and joints (i.e., fully mortared or dry head-joints). The improvement of the current codified strength expressions and the development of new ones, that may consider all possible mechanisms and better identify the actual failure mode, is envisaged; for example, masonry with blocks and unfilled/mortar pocket head-joints surely need further investigation. Moreover, a consistent definition of performance levels and corresponding values of drift limits in relation with the effective failure mode is also of paramount importance for a reliable evaluation of the in-plane response of masonry walls, in particular when dealing with design/assessment approaches of URM buildings using non-linear analyses. The future challenge appears to be a reliable definition of the basic design parameters to be provided by the building codes, primarily the strength criteria and drift limits, diversified for the different masonry structural systems, each formulated as a function of appropriate failure mechanisms specific for that masonry typology which are, in their turn, not only depending on the level of compression, on the geometry and on the boundary conditions of the walls, but also on the materials used for the units and on the types of blocks and joints.

ACKNOLEDGEMENTS

This research has been carried out at the University of Pavia and EUCENTRE and it has been partially funded by the Executive Project DPC-RELUIS 2013-2016 and by ASSOPLAN s.c.r.l.. The financial support received is gratefully acknowledged.

REFERENCES

[1] Magenes G., Morandi P., Penna A. (2008). *Test results on the behaviour of masonry under static cyclic in plane lateral loads*. Deliverable D7.1c, ESECMaSE Project, www.esecmase.org.

[2] Magenes G., Calvi G.M. (1992). *Cyclic behaviour of brick masonry walls*. Proc. of the 10th World Conference on Earthquake Engineering, Madrid.

[3] Anthoine A., Magonette G., Magenes G. (1995). *Shear-compression testing and analysis of brick masonry walls*. Proc. of the 10th European Conference on Earthquake Engineering, Vienna.

[4] Abrams D.P., Shah N. (1992). *Cyclic load testing of unreinforced masonry walls*. U.S. Army Research Office.

[5] Bosiljkov V., Page A., Bokan-Bosiljkov V., Žarnić R. (2003). *Performance based studies of in-plane loaded unreinforced masonry walls*. Masonry International, Vol. 16, No. 2, 39-50.

[6] Manzouri T., Schuller M.P., Shing P.B., Amadei B. (1995). *Repair and retrofit of unreinforced masonry structures*. Earthquake Spectra, Vol. 12, No. 4, 903-922.

[7] Bosiljkov V., Tomaževič M. (2004/2006). *Optimization of shape of masonry units and technology of construction for earthquake resistant masonry buildings.* Research report (part I and III), ZAG, Ljubljana.

[8] Zilch K., Finck W., Grabowski S., Schermer D., Scheufler W. (2008). *Test results on the behaviour of masonry under static cyclic in plane lateral loads*. Deliverable D7.1.b, ESECMaSE Project, www.esecmase.org.

[9] Fehling E., Stuerz J., Emami A. (2007). *Test results on the behaviour of masonry under static (monotonic and cyclic) in plane lateral loads*. Deliverable D7.1a, ESECMaSE Project, www.esecmase.org.

[10] Ötes A., Löring S. (2003). *Tastversuche zur identifizierung des verhaltensfaktors von mauerwerksbauten für den erdbebennachweis*. Technical report, University of Dortmund.

[11] Penna A., Mandirola M., Rota M., Magenes G. (2015). *Experimental assessment of the in-plane lateral capacity of autoclaved aerated concrete (AAC) masonry walls with flat-truss bed-joint reinforcement*. Construction and Building Materials, Vol. 82, 155-166.

[12] Rosti A., Penna A., Rota M., Magenes G. (2016). *In-plane cyclic response of low-density AAC URM walls*. Material and Structures, Vol. 49, No. 11, 4785-4798.

[13] Costa A., Penna A., Magenes G. (2011). *Seismic performance of autoclaved aerated concrete (AAC) masonry: from experimental testing of the in-plane capacity of walls to building response simulation*. Journal of Earthquake Engineering, Vol. 15, No. 1, 1-31.

[14] Petry S., Beyer K. (2014). *Influence of boundary conditions and size effect on the drift capacity of URM walls*. Engineering structures, Vol. 65, 76-88.

[15] Modena C., Da Porto F., Garbin E. (2005). *Ricerca sperimentale sul comportamento di sistemi per muratura portante in zona sismica*. Report, University of Padova.

[16] Frumento S., Magenes G., Morandi P., Calvi G.M. (2009). *Interpretation of experimental shear tests on clay brick masonry walls and evaluation of q-factors for seismic design*. Eucentre Research Report 2009/02, IUSS Press, Pavia.

[17] Morandi P., Albanesi L., Magenes G. (2013). *In-plane experimental response of masonry walls with thin shell and web clay units*. Proc. of the Vienna Congress on Recent Advances in Earthquake Engineering and Structural Dynamics 2013, Vienna.

[18] Morandi P., Albanesi L., Magenes G. (2014). *URM walls with thin shell/web clay units and unfilled head-joints: cyclic in-plane tests*. Proc. of the Second European Conference on Earthquake Engineering and Seismology, Istanbul.

[19] Fehling E., Stürz J. (2008). *Experimentelle untersuchungen zum schubtragverhalten von porenbetonwandscheiben*. Report, University of Kassel.

[20] Salmanpour A.H., Mojsilović N., Schwartz J. (2015). *Displacement capacity of contemporary unreinforced masonry walls: an experimental study*. Engineering Structures, Vol. 89, 1-16.

[21] Morandi P., Albanesi L., Magenes G. (2015). *Prestazioni sismiche di pannelli murari in blocchi di laterizio a setti sottili soggetti a test ciclici nel piano*. Atti del XVI Convegno ANIDIS - L'ingegneria Sismica in Italia, L'Aquila [in Italian].

[22] Graziotti F., Rossi A., Mandirola M., Penna A., Magenes G. (2016). *Experimental characterization of calcium-silicate brick masonry for seismic assessment*. Brick and Block Masonry: Trends, Innovations and Challenges - Proceedings of the 16th International Brick and Block Masonry Conference, IBMAC 2016, 1619-1628.

[23] Graziotti F., Tomassetti U., Rossi A., Marchesi B., Kallioras S., Mandirola M., Fragomeli A., Mellia E., Peloso S., Cuppari F., Guerrini G., Penna A., Magenes G. (2016). *Shaking table tests on a full-scale clay-brick masonry house representative of the Groningen building stock and related characterization tests*. Report EUC128/2016U, Eucentre, Pavia.

[24] Mallardo V., Malvezzi R., Milani E., Milani G. (2008). Seismic vulnerability of historical masonry buildings: a case study in Ferrara. Engineering Structures, 30(8), 2223-2241.

[25] Crowley H., Polidoro B., Pinho R., van Elk J. (2017). Framework for developing fragility and consequence models for local personal risk. Earthquake Spectra, 33.4: 1325-1345.

[26] Kallioras S., Morandi P., Penna A., and Magenes G. (2018). *Seismic performance assessment of three modern masonry buildings struck by the 2012 Emilia earthquake.* Proc. of the 10th International Masonry Conference, Milan, July 9-11, 2018.

[27] Adam J.M., Brencich A., Hughes T.G., Jefferson T. (2010). Micromodelling of eccentrically loaded brickwork: study of masonry wallettes. Eng Struct 2010;32(5):1244–51.

[28] Gabor A., Ferrier E., Jacquelin E., Hamelin P. (2006). Analysis and modelling of the in-plane shear behaviour of hollow brick masonry panels. Constr Build Mater 2006;20:308–21.

[29] Magenes G., Manzini C.F., Morandi P., Remino M., Bolognini D. (2006). *SAM II, Software for the Simplified Seismic Analysis of Masonry buildings*. University of Pavia and EUCENTRE.

[30] Lagomarsino S., Penna A., Galasco A., Cattari S. (2013). *TREMURI program: an equivalent frame model for the nonlinear seismic analysis of masonry buildings*, Engineering Structures, 56, pp. 1787-1799, Elsevier, ISSN: 0141-0296, http://dx.doi.org /10.1016/j.engstruct.2013.08.002.

[31] Augenti N., Parisi F., Acconcia E. (2012*). MADA: online experimental database for mechanical modelling of existing masonry assemblages.* Proc. of the 15th World Conference on Earthquake Engineering, Lisbon.

[32] Salmanpour A.H., Mojsilović N., Schwartz J. (2013). *Deformation capacity of unreinforced masonry walls subjected to in-plane loading: a state-of-the-art review.* International Journal of Advanced Structural Engineering, Vol. 5, 22.

[33] Gams M., Triller P., Lutman M., Snoj J. (2016). *Seismic behaviour of URM walls: analysis of a database.* Brick and Block Masonry: Trends, Innovations and Challenges - Proceedings of the 16th International Brick and Block Masonry Conference, IBMAC 2016, 1593-1600.

[34] Vanin F., Zaganelli D., Penna A., Beyer K. (2017). *Estimates for the stiffness, strength and drift capacity of stone masonry walls based on 123 quasi-static cyclic tests reported in the literature.* Bulletin of Earthquake Engineering, Vol. 15, No. 12, 5435-5479.

[35] Morandi P., Albanesi L., Graziotti F., Li Piani T., Penna A., Magenes G. (2018). Dataset on in-plane experimental response of URM piers with bricks and blocks; available at the url: https://drive.google.com/open?id=14hnlBUtTTzvtagF9VysYCtxTkq0W-A-u

[36] EN 772-1 (2011). *Methods of test for masonry units - Determination of compressive strength.*

[37] EN 998-2 (2010). *Specification for mortar for masonry - Masonry mortar.*

[38] CEN (2005). *Eurocode 6 - Design of masonry structures - Part 1-1: Common rules for reinforced and unreinforced masonry structures.* EN 1996-1-1:2005, Brussels.

[39] EN 1052-1 (2001). *Methods of test for masonry - Determination of compressive strength.*

[40] EN 1052-3 (2007). *Methods of test for masonry - Determination of initial shear strength*.

[41] D.M. 17/01/2018. *Norme Tecniche per le Costruzioni (NTC 2018).* Gazzetta Ufficiale, n. 42 del 20/02/2018, Supplemento ordinario n.8 [in Italian].

[42] Magenes G., Calvi G.M. (1997). *In-plane seismic response of brick masonry walls*. Earthquake Engineering and Structural Dynamics, Vol. 26, 1091-1112.

[43] Jacobsen L.S. (1960). Damping in composite structures. In: Proceedings of 2nd World Conference on Earthquake Engineering, vol 2. Tokyo and Kyoto, Japan, pp 1029–1044.

[44] Turnšek V., Čačovič F. (1971). *Some experimental results on the strength of brick masonry walls.* Proc. of the 2nd International Brick Masonry Conference, Stoke-on-Trent.

[45] Benedetti, D., Tomaževič, M. (1984). "Sulla verifica sismica di costruzioni in muratura". *Ingegneria Sismica*, Vol. I [in Italian].

[46] D.M. 14/01/2008. *Norme Tecniche per le Costruzioni (NTC 2008).* Gazzetta Ufficiale, n. 29 del 14/02/2008, Supplemento ordinario n.30 [in Italian].

[47] CEN (2005). *Eurocode 8 - Design of structures for earthquake resistance - Part 3: Assessment and retrofitting of buildings.* EN 1998-3:2005, Brussels.

[48] *Circolare Ministeriale del 02/02/2009 n.617, 2009 - Istruzioni per l'applicazione delle Nuove norme tecniche per le costruzioni* [in Italian].